LC-DET-2004-031

The Beam Energy Spectrometer at the International Linear Collider

V.N. Duginov[3], H. Henke[4], K. Hiller[2], A. Liapine[4,2], T.N. Mamedov[3], I.N. Meshkov[3], N.A. Morozov[3], H.J. Schreiber[2], E.M. Syresin[3], I.V. Titkova[3], K. Trützschler[2] and N. Walker[1]

[1] Deutsches Elektronen-Synchrotron DESY, D-22607 Hamburg, Germany

[2] Deutsches Elektronen-Synchrotron DESY, D-15703 Zeuthen, Germany

[3] Joint Institute for Nuclear Research Dubna, R-141980 Dubna, Russia

[4] TU Berlin, Fachgebiet für Theoretische Elektrotechnik, D-10587 Berlin, Germany

Abstract

This note describes an upstream beam energy spectrometer for the linear e^+e^- collider based on the superconducting RF technology. The spectrometer is proposed to perform single-bunch measurements of the beam energy between 45 and 400 GeV with a precision of $\Delta E_b/E_b \simeq 1\cdot 10^{-4}$ or better. It consists of one analyzing and two ancillary bending magnets with a series of high-precision beam position monitors (BPMs). A compact option of the spectrometer with a bending angle of 1 mrad is proposed, with a position in the BDS which can be optimized for tolerable emittance dilution in the bending plane. Warm magnets with ferromagnetic cores are suggested. The field integral uncertainty is required to be $\Delta B/B \simeq 2 \cdot 10^{-5}$, which can be realized with proven techniques. RF cavity BPMs with a novel coupling scheme and dedicated read-out electronics can achieve 100 nm position resolution. Survey, alignment and monitoring of the spectrometer components are performed using state-of-the-art alignment and stabilization techniques. Control of BPM electronics, magnetic field drifts and ground motion have to be carefully accounted for. A spectrometer located close to the IP is also shortly discussed. This option is however not recommended, in particular for the zero-crossing angle design of a TESLA-like linac.

1 Introduction

A full exploitation of the physics potential of an high-energy e^+e^- linear collider, as proposed by e.g. the TESLA collaboration [1], must aim for absolute precise beam energy measurements to control the collision energy $\sqrt{s}$, the differential dependence of the luminosity on energy ($d\mathcal{L}/d\sqrt{s}$), and the relationship between these two quantities and the energy of a single beam (E_b). For example, accurate knowledge of $\sqrt{s}$ at e^+e^- colliders has always been a tremendous advantage for performing precise measurements of particle masses. At circular machines, for example at LEP, the precise energy determination using resonant depolarization allowed an exquisite measurement of the Z boson mass to an uncertainty of 2 MeV or 23 ppm. At a future linear collider (LC), however, the resonance depolarization technique cannot be applied and different methods have to be employed. As discussed below, the physics requirements anticipated level of precision should be basically attainable by beam-based magnetic spectrometers. The deflection of a charged particle traversing a magnetic field is a well established method for measuring a particle's momentum. High-precision beam position monitors (BPMs) combined with a precise knowledge of the integrated magnetic field (B) of a bending magnet are the basic components of the spectrometer located upstream of the interaction point (IP).

The quantity of basic interest is, however, the energy of the two beams at the IP. Since a precise energy measurement at the interaction point is difficult to achieve or even excluded, the location of the measurement should be chosen such that effects from the beam transport are either negligible or small and well quantified. In particular, emittance growth should be minimized or mitigated to an acceptable level. Other important factors relate to dedicated alignment procedures, control of the BPM electronics, B-field shifts and ground motion, to temperature stabilization of the magnets and the BPMs, to the level of radiation background, to the technical infrastructure, to an implementation of a possible complementary beam energy determination and accessibility of the site chosen.

Also important will be a beam energy measurement and its control after the IP. This possibility, which would in principle permit to study beam-beam effects experimentally, has to be independently investigated and is not within the scope of this study.

An in-line BPM spectrometer using button monitors was successfully operated at LEP2 to cross check the energy scale for W mass measurements [2]. A relative error on the center-of-mass energy determination for the majority of LEP2 running of 120-200 ppm had been achieved. This precision was possible due a precise map of the magnetic field and careful calibration using resonant depolarization at the Z pole. The limiting systematic errors have come from the stability of the BPM electronics.

The report is organized as follows. In Sect. 2 physics requirements are summarized. Sect. 3 describes the basic properties of a possible spectrometer, followed by some discussion for a suitable location within the TESLA beam delivery system [1] as an example. Sect. 3.4 describes the proposed magnets, including magnet tolerances, temperature stabilization, B-field measurement options in the laboratory and in situ. It is followed by the discussion on the beam position monitors in Sect. 3.5. The basic behaviour of RF-cavity BPMs and a possible design including the read-out electronics are described. Results of first measurements using a test bench and tests with beam are also presented. Sect. 3.6 is devoted to stabilization and alignment issues and the control of the spectrometer. Preliminary cost estimates are given in Sect. 4. Sect. 5 contains the summary and conclusions.

2 Physics Requirements

There are two main types of physics analyses which depend significantly upon precise knowledge of the collision energy $\sqrt{s}$. The first is the measurement of the threshold cross-section for a particular final state in dependence on $\sqrt{s}$ which is sensitive to the mass of the particles produced. The second is the reconstruction of particle resonances in the continuum where kinematical constraints may be used to improve the mass resolution. In both cases, the relative uncertainty on E_b translates directly into an overall scale error of the extracted particle mass.

The canonical example for a cross-section scan is the measurement of the top quark mass, M_{top}, by scanning the $t\bar{t}$ threshold at $\sqrt{s} \sim 350$ GeV. An accumulated luminosity of 10 fb^{-1} at several energies across the $t\bar{t}$ threshold results to a statistical uncertainty of about 40 MeV [3]. Accounting also for a theoretical error of similar size, results to a relative precision demand on E_b of 10^{-4} or 100 ppm. This beam energy uncertainty of 20 MeV on M_{top} is well matched to the total accuracy on the top mass expected to be smaller than 100 MeV.

As discussed in ref. [4], precise knowledge of the top quark mass has very strong impacts on predictions of electroweak precision observables within e.g. the Standard Model (SM) and its minimal supersymmetric extension (MSSM). Stringent internal consistency checks of both models are only possible with an accuracy of $\Delta M_{top} \leq 100$ MeV.

An example of a continuum measurement is the determination of the mass of the SM Higgs boson, M_H, by direct reconstruction of the Higgs-strahlung process $e^+e^- \to HZ$, with Higgs decays into two jets, leptons or bosons. Since the SM Higgs boson mass is a fundamental parameter of the theory, its precise measurement is very important. Once M_H is fixed, the profile of the Higgs particle is uniquely determined in the SM. Using a procedure similar to the W mass measurements at LEP [5], an uncertainty of the beam energy translates directly into a measurement error of the Higgs mass, ΔM_H, according to

$$\frac{\Delta M_H}{M_H} = \frac{\Delta E_b}{E_b} \quad . \tag{1}$$

A precision of 10^{-4} for the beam energy results to ΔM_H of about 12 MeV for a light Higgs boson which matches best with an error of 40 to 50 MeV expected from Higgs mass reconstruction [6] in the continuum.

Such an accuracy for the Higgs boson mass, together with the anticipated precision on M_{top}, allows for example detailed studies and internal consistency checks of the MSSM Higgs and the scalar top sector [4]. In particular, confronting the theoretical prediction for M_H with a precise measurement of the Higgs mass allows to obtain sensitive constraints on the model parameters.

For running above the $t\bar{t}$ threshold a relative precision on E_b of 100 to 200 ppm appears to be adequate. At the moment no clear apparent physics analysis exists which points to an improved beam energy determination. An example could certainly be a scenario where weakly interacting quasi-stable particles are pair-produced, and a threshold scan with high luminosity would aim to measure their mass better than 100 ppm.

For analyses proposed at lower energies two examples are reviewed here.

Measuring the mass of the W boson, M_W, by means of a threshold scan or by less-favored 2-jet mass reconstruction in the continuum is only interesting, if the total error can be reduced to about 5 MeV [7] [1]. This requires a precision on $\Delta E_b/E_b$ of 30 to 40 ppm or an absolute

[1] The error on M_W is expected to be close to 15 MeV at the time when the LC is commissioned.

beam energy uncertainty of $\Delta E_b \sim 3$ MeV, and likely an alteration in accelerator parameters to control $d\mathcal{L}/d\sqrt{s}$.

For measurements of the weak mixing angle $sin^2\theta_{eff}$ from left-right asymmetry measurements, precise information on E_b is necessary to correct the measured value back to the theoretical Z pole value [8]. The required precision relative to the Z pole depends on the experimental uncertainty attainable for the beam polarization. If only electrons are polarized with 90% polarization, $\Delta P_e/P_e$=0.25% and 50 million accumulated events a precision of ± 0.00005 on $sin^2\theta_{eff}$ may be possible if $\Delta E_b/E_b$ does not exceed 110 ppm. With both beams polarized (90%,50%, an effective polarization error of $\Delta P_{eff}/P_{eff}$=0.10% and 100 million events for example), the beam energy must be known to about 2 MeV or 40 ppm to obtain an error of ± 0.00002 on $sin^2\theta_{eff}$.

We note that there may be also the desire to re-scan the Z lineshape. This, however, would require $\Delta E_b/E_b \sim$ (5-1) ppm, which is probably out of range of a BPM-based spectrometer.

Hence, to realize fully the potential of a LC for significantly improved measurements on the W mass and $sin^2\theta_{eff}$ running at M_Z (GigaZ), very precise beam energy information under optimized running conditions is essential.

A further motivation for a dedicated assessment of E_b consists in the following. The integrated luminosity, $\int \mathcal{L}dt$, which effectively normalizes cross-section measurements, is proportional to the square of the beam energy [2]. Should a LC beam energy be in error, not only the uncertainties on cross-sections would be underestimated, but their central values would be incorrectly normalized and, hence, mismeasured. It is, however, a non-trivial task to relate E_b measurements from the spectrometer to $\sqrt{s}$, the effective center-of-mass energy, at the collision point due to beam disruption and beamstrahlung effects [9].

It should be stressed that the requirements on ΔE_b listed above are targets which are required to carry out the physics program at an high-energy e^+e^- linear collider. Compared to results so far achieved from existing techniques, a factor of 5 to 10 improved energy determination is needed. This is an essential technical challenge, where solutions to nanometer-scale stability and resolution will be necessary. In conjunction with acolinearity measurements of forward Bhabha scattering, physics analyses using radiative return events, $e^+e^- \rightarrow Z\gamma$, or Z- and W-pair production, relying on precise Z respectively W mass information, energy calibration as needed for physics at the linear collider should be achievable.

3 The Spectrometer

3.1 General Considerations

The concept of the energy measurement spectrometer is based on the determination of the bending angle of a charged particle through a magnetic dipole field. The particle energy is proportional to the integrated field and inversely proportional to the bending angle Θ:

$$E_b = \frac{c \cdot e}{\Theta} \int\limits_{magnet} Bdl \quad , \tag{2}$$

where c is the speed of light and e the charge of the particle. The analyzing magnet is supplemented by two ancillary magnets to compensate the bend of the spectrometer magnet.

[2]Usually, small-angle Bhabha scattering events, $e^+e^- \rightarrow e^+e^-$, recorded in forward calorimetry together with the theoretically well-know 1/s dependent Bhabha cross-section determine $\int \mathcal{L}dt$.

The deflection angle is measured from the beam trajectories on both sides of the spectrometer magnet in the field free arms using RF cavity beam position monitors. Such monitors can potentially achieve precisions on the transverse beam position approaching few tens of nanometers.

Measurements at different nominal beam energies are proposed to be performed at constant bending angle Θ by adjusting the field strength B of the magnets.

The beam position monitors are designed to have a fast response performing bunch-by-bunch measurements up to $\sqrt{s}$ = 800 GeV with a bunch spacing of ∼170 nsec. This would allow to recognize variations of the beam energy within a bunch train (or pulse) of about 4880 bunches.

The BPM-based energy spectrometer will be located upstream of the IP. Provisions must be made in the overall accelerator design to provide adequate beamline space in the range of 30 to 50 m.

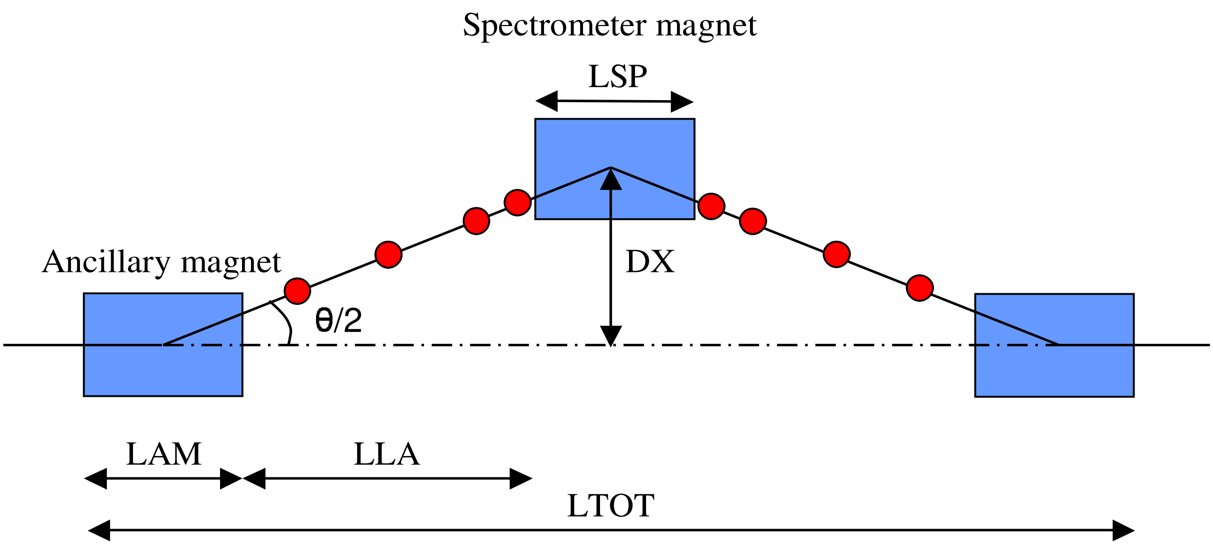

Figure 1: Schematic layout of the magnetic spectrometer. The circles indicate the beam position monitors (BPMs).

3.2 Basic Spectrometer Parameters

A primary constraint for the design of the energy spectrometer is the emittance growth due to synchrotron radiation from the magnets of the spectrometer. It has to be kept to an acceptable limit. Emittance dilution in the bending plane, ε_x, for a chicane as indicated in ref.[1] has been estimated of 3 to 4% at 400 GeV beam energy, which we consider as tolerable [3]. It has however to be demonstrated that any vertical ε_y growth is small enough to be acceptable. For the following discussion we assume tolerable emittance dilution for a spectrometer as sketched in [1].

The basic layout of the magnetic chicane is shown in Fig. 1. Key parameters which determine the precision of the beam energy are the length of the lever arms L_{LA}, the position accuracy σ_{BPM} of the BPMs, their number per lever arm and the precision on the integrated field of the analyzing magnet, $\Delta B/B$. We assume in the following symmetrically arranged and equidistant BPMs between the magnets, a nominal beam energy of 250 GeV, a bending angle of 1 mrad, a perfect aligned spectrometer and ideal beam conditions. We aim to provide a set of parameters

[3] At smaller energies emittance growth will be substantially reduced or negligible since it scales with the sixth power of E_b.

to ensure a relative uncertainty of $\Delta E_b/E_b = 5 \cdot 10^{-5}$. This figure of merit corresponds to an absolute energy uncertainty of 12.5 MeV at $E_b = 250$ GeV and of 2.3 MeV for running at the Z pole, which are in accordance with most of the physics requirements as discussed in Sect.2.

The dependence of the energy resolution $\Delta E_b/E_b$ as function of the parameters under discussion can be expressed as

$$\Delta E_b/E_b = \sqrt{(\Delta B/B)^2 + 2f(N) \cdot (E_B \cdot \sigma_{BPM}/c \cdot L_{LA} \cdot B)^2} \quad , \tag{3}$$

where f(N) depends on the number N of BPMs per lever arm:

$$f(N) = N(N-1)^2/(\sum_{i=1}^{N} i^2 - (\sum_{i=1}^{N} i)^2) \quad . \tag{4}$$

Fig. 2 illustrates the energy resolution as function on L_{LA}, σ_{BPM}, $\Delta B/B$ and N. As expected, strong dependencies are observed on the position resolution of the BPMs and the length of the lever arm. Magnetic field errors become more important at small σ_{BPM} values. The $\Delta E_b/E_b$ dependence on the number of monitors per lever arm is rather weak. We fix them to at least three in the following. Two BPMs would basically fix a straight line, but three allow a relative BPM calibration by means of the others in each arm separately. It is advantageous to add to the three equidistant BPMs a fourth one very close to (or within the) fringe field of the spectrometer magnet (Fig. 1). Due to strong local variations of the fringe field this monitor allows a precise position measurement in this field region and could improve integrated B-fields values. Assuming for $L_{LA} = 10$ m, an integrated B-field uncertainty of $\Delta B/B = 2{\cdot}10^{-5}$ and an absolute BPM position accuracy of 200 nm, $\Delta E_b/E_b = 5 \cdot 10^{-5}$ is within reach. Additional BPMs upstream and downstream of the chicane would constrain external particle trajectories, so that some more empty space is needed.

A deflection angle of $\Theta = 1$ mrad together with $L_{LA} = 10$ m results to a maximum beam offset $D_x = 5.8$ mm (Fig. 1).

A beam energy spectrometer with such parameters possesses the following advantages:

- sufficient field free drift space of 10 m for both lever arms;
- a total length for the spectrometer of some 25 m;
- due to small L_{tot}, a common support girder for all spectrometer components can be considered minimizing ground motion disturbing effects;
- relative moderate BPM position resolution requirements;
- integrated B-field precision attainable with present state-of-the-art techniques.

For an ILC beam delivery system (its evaluation started recently) design constraints due to possible emittance growth (for beam energies up to 1 TeV) will drive the final parameters of the magnetic spectrometer. For example, the size of the bending angle or the length of the magnets or both need to be reconsidered, which in turn results to some reoptimization of the spectrometer as a whole.

If detailed studies on such a compact large-angle spectrometer would result in an intolerable emittance growth, a small-angle spectrometer has to be placed close to the IP upstream of the final doublets. Here, intolerable beam size blow-up can be avoided by reducing the deflection angle of the spectrometer by typically a factor of ten, i.e. $\Theta = 0.1$ mrad. Fig. 3 summarizes possible key parameters to maintain $\Delta E_b/E_b = 5 \cdot 10^{-5}$ for this case. As can be seen, the demand

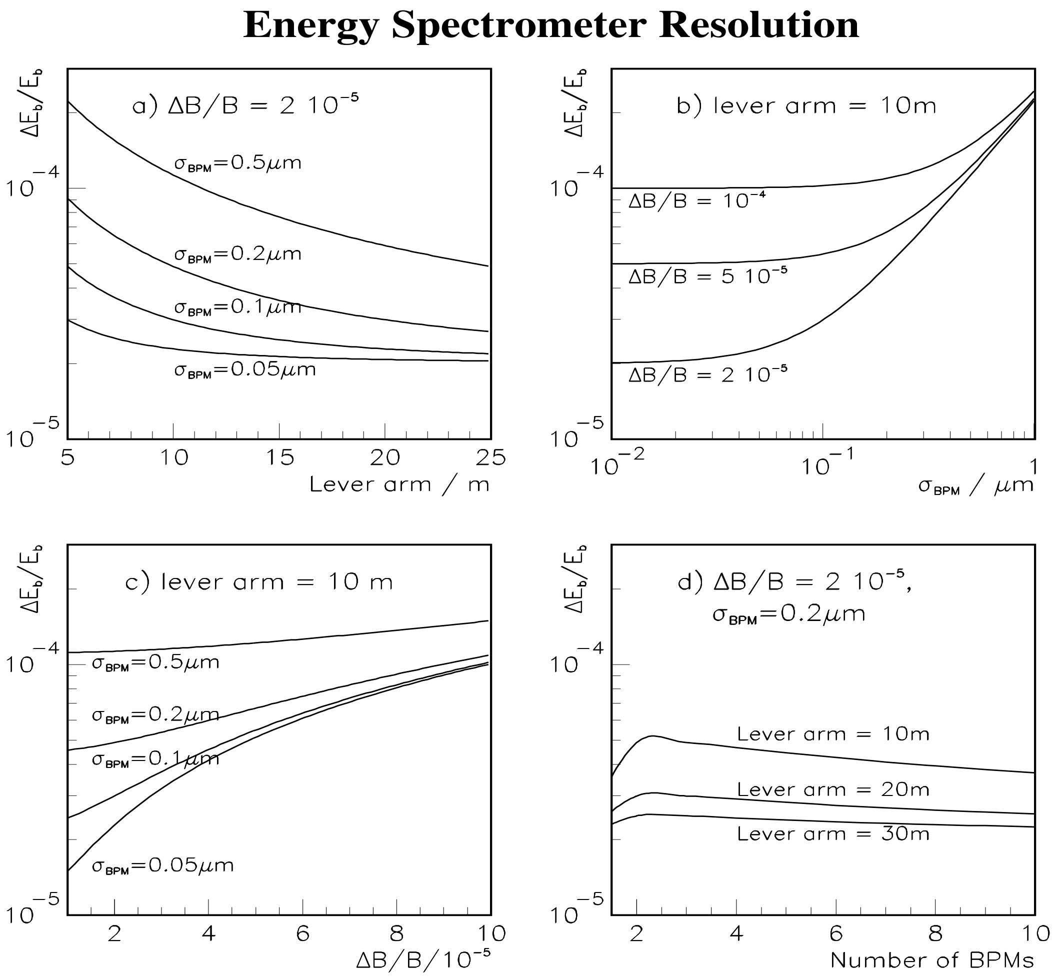

Figure 2: Energy resolution, $\Delta E_b/E_b$, versus lever arm length, BPM resolution, magnetic field error and number of BPMs per lever arm, for fixed deflection angle $\Theta = 1$ mrad. Top left: $\Delta B/B = 2{\cdot}10^{-5}$, N = 3 and $\sigma_{BPM} = 0.5$ to 0.05 μm. Top right: $L_{LA} = 10$ m, N = 3 and $\Delta B/B = 10^{-4}$ to $2{\cdot}10^{-5}$. Bottom left: $L_{LA} = 10$ m, N = 3 and $\sigma_{BPM} = 0.5$ to 0.05 μm. Bottom right: $\Delta B/B = 2{\cdot}10^{-5}$, $\sigma_{BPM} = 0.2$ μm and $L_{LA} = 10$ to 30 m.

can be preserved e.g. for an absolute BPM position accuracy of 50 nm and a lever arm of $L_{LA} \simeq 22$ m or for $\sigma_{BPM} = 100$ nm and a lever arm of some 45 m. The latter option with a total spectrometer length of about 100 m might be in conflict with beam line optics elements and will not be further discussed. Only the possible spectrometer design with a total length of about 50 m is shortly considered as a complementary but diffident spectrometer option located close to the IP.

3.3 Suitable Spectrometer Locations

The beam delivery system (BDS) transports the beam from the exit of the linac to the IP. In the following, we discuss, as an example, some details for a possible location of the spectrometer within the BDS as proposed by the TESLA collaboration [1]. Fig. 4 shows the layout of the BDS for the electron side, with indications of the location for the positron source and the fast emergency extraction line [4]. The IP is located at z = 1759 m.

[4]The e^+ delivery system is very similar except for the positron source.

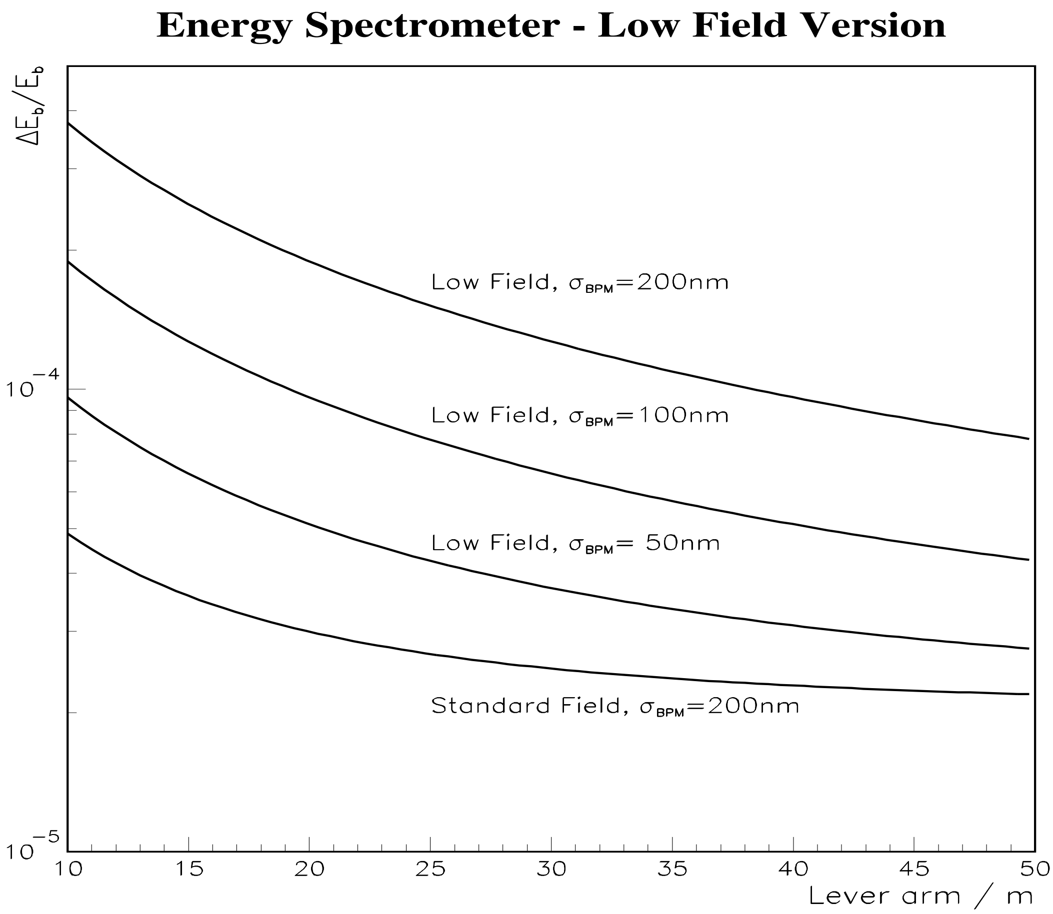

Figure 3: Energy resolution, $\Delta E_b/E_b$, versus lever arm length, for $\Delta B/B = 2{\cdot}10^{-5}$, N = 6 and some σ_{BPM} values between 50 and 200 nm. For comparison the large-angle resolution curve is also shown for the default key parameters.

Part II of the TESLA TDR [1] describes the magnetic lattice and the optics of the modules which specify the functionality of the BDS. It starts with the e^+ source undulator, followed by the switch-yard arc to provide beams to a second IP and the magnetic energy spoiler (ECOL) which 'blows up' the beam to collimate particles with large off-energies. These modules are not suitable to house a 25 m long energy spectrometer.

The collimation and diagnostic section (CDS, start at z = 670 m) possesses a repetitive lattice where a series of spoilers and absorbers to collimate the beam halo. The collimation is performed at intervals of 45^o phase advance, at locations of relatively large beam size ($\sigma_{x,y}$ = 127, 7 μm at 250 GeV). In this section, the beamline is aligned with the collision axis, except for a parallel offset of about 60 cm, which separates the beam from beamstrahlung products of the other beam. Upstream of the final telescope (FT) are two dispersive sections referred as horizontal (HCCS) and vertical (VCCS) chromatic correction sections, where pairs of strong sextupoles are used to correct the strong chromaticity of the final doublet. Basically, several adequate locations exist for well suited energy measurements within the diagnostic section. It is however advantageous to position the spectrometer after collimation of halo particles and absorption of scattered particles.

The location proposed for the spectrometer within the collimation and diagnostic section at z = 1015 m is optimal with respect to the free space available. In addition, the beam has relatively small transverse sizes (σ_x = 15...44 μm, σ_y = 2...5 μm) and is well collimated (the last spoiler is 55 m upstream). The collimation system (spoilers followed by thick absorbers) physically scraps the halo particles off the beam, which is in favour of the robustness of the BPM measurements. Installation of additional background absorption devices and muon depletion toroids [12] upstream of the spectrometer would also favour this position.

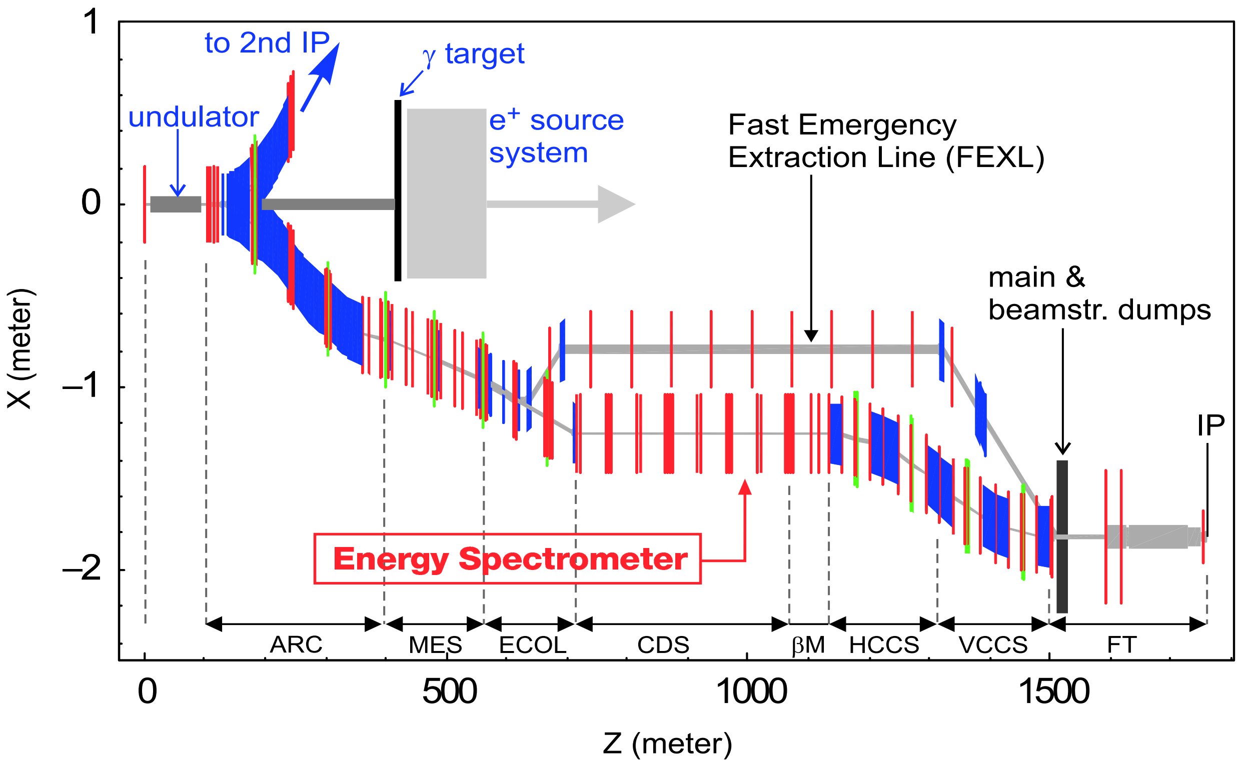

Figure 4: Basic geometry of the primary e^- BDS from linac to IP.

Alternatively, the small-angle spectrometer option with the length of 50 m could be located into the final telescope (FT) either at z = 1628...1707 m or at z = 1518...1591 m. Here, between the beam dump for the opposite beam and the final quadrupoles, free drift space more than needed exists. In this region, the beam from the linac is transported to the IP and the strongly disrupted beam from the IP is delivered to the dumps. Both beams are accommodated in a common tube with continously increasing aperture [5]. Such a layout for the beam line in which a BPM-based spectrometer might be incorporated is for several reasons not suitable for precise beam energy monitoring. Large aperture beam pipes would require cavity monitors with a diameter about three times larger together with correspondingly scaled waveguides (see Sect. 3.5). Such BPMs render significantly beam position measurements with 50 nm precision due to larger fabrication tolerances. Also, dedicated shielding of the monitors and the C-shaped spectrometer magnets (Sect. 3.4) from beamstrahlung photons requires substantial R&D, with uncertain success. In addition, if the time difference between the incoming beam and the disrupted beam or the beamstrahlung products in the BPM is smaller than the monitor damping time, the BPM response is disturbed. Very fast BPMs are needed for such an option.

In summary, the present TDR design of the beam extraction line based on the TESLA zero-crossing concept is not suitable to maintain precise beam energy measurements using a BPM-based spectrometer at the near-IP location. In the case of intolerable total emittance dilution for the compact version of the spectrometer, the small-angle near-IP option will be discussed under the assumption of a non-zero crossing angle design for the linear collider. In

[5]At the spectrometer positions suggested the TDR beam pipe diameters are 140 respectively 200 mm.

this way a small beam pipe aperture ($\sim$20 mm) can be maintained up to the detector. However, whatever option for the energy spectrometer is suitable, any re-evaluation of the BDS within the International Linear Collider framework should account for the energy spectrometer related arguments.

3.4 The Magnets

The proposed energy spectrometer concept of the LC should be realized by utilizing warm magnets with ferromagnetic core. Advantages of this proposal are:

- high magnetic system reliability and straight forward preparation for operational conditions;
- simple access to the magnets and equipment alignment;
- short time realization for modeling of spectrometer components as well as the whole spectrometer;
- simple and low cost magnet designs, manufacturing and operation.

However, in the case of warm magnets some concerns require additional efforts:

- temperature stabilization of the magnet;
- adjustment of the magnetic zero-field;
- elimination of hysteresis effects.

3.4.1 Requirements, Prototypes and Total Scheme

Magnet spectrometers for precision energy measurements were developed at LEP [13], [14], [15], [16] and SLC [17], [18], [19]. At CEBAF, a high-quality magnet was proposed for the ARC project [20], [21], [22] to be utilized as reference dipole for accurate beam energy determination.

The setup for the energy spectrometer, as discussed in Sect. 3.2, consists of two deflection magnets and one analyzing magnet. The field integral of the analyzing magnet has to be mapped to a resolution of $\Delta \int Bdl / \int Bdl \lesssim 2 \cdot 10^{-5}$ for beam energies between 45 and 400 GeV. The deflection angle in the spectrometer magnet is proposed to be 1 mrad for all beam energies anticipated. The basic parameters of the analyzing magnet proposed are collected in Tab. 1 and compared with similar magnets developed at SLC, LEP and CEBAF. The overall objective of the field integral uncertainty $\Delta \int Bdl / \int Bdl \sim 2 \cdot 10^{-5}$ might be achievable by accounting for

- the experiences obtained at SLC, LEP and CEBAF;
- a similar design and manufacturing tolerances for the ILC magnets;
- two independent techniques for field measurements in the laboratory as well as in situ;
- temperature measurements, excitation current stabilization and demagnetization procedures for the spectrometer magnet in situ.

The basic layout of the spectrometer magnet system is presented in Fig. 5 (half part because of the system symmetry). If the magnets are switched off, the beam continues to move along its ballistic path. When the magnets are powered, the beam is deflected by 0.4 mm from its original path at the exit of the first ancillary magnet. The beam offset increases to 5.4 mm at the analyzing magnet after a drift of 10 m and achieves a maximum of 5.8 mm in the center of

	SLC	LEP	CEBAF	ILC (Proposal)
Energy E (GeV)	42 - 50	40 - 100	0.5 - 7	45 - 400
Rel. accuracy of energy measurement ΔE/E	5×10^{-4}	1×10^{-4}	1×10^{-4}	1×10^{-4} 5×10^{-4}
Bending angle (mrad)	18.286	3.75		1
Field range (T)	0.88-1.1	0.086-0.216	0.04-0.6	0.05-0.44
Field integral (T·m)	2.56-3.05	0.5-1.242	0.12-1.8	0.15-1.33
Error of the field integral (relative)	7×10^{-5}	3×10^{-5}	1×10^{-5}	2×10^{-5}
Magnet iron length (m)	2.5	5.75	3	3
Eff. magnet length (m)				3.045
Gap height (mm)	31.7	100	25.4	35
Magnet type	H	C	C	C
Laboratory $\int$ B·dl measurement technique	Moving were, moving probe (NMR, Hall)	Moving probe (NMR, Hall), search coil	NMR probe, 2 search coils	Moving probe (NMR, Hall), search coil
Operational $\int$ B·dl measurement technique	Flip coil fixed probes (NMR)	Fixed probes (NMR)		Fixed probes (NMR), moving wire
Max. energy loss due to synchrotron rad. (MeV)		3.55		0.02-120

Table 1: Basic parameters of spectrometer magnets.

the system. Due to a transverse shift of the magnetic field uniformity region with respect to the center of the magnets, the pole axis of the ancillary magnets is off by 4 mm from the beam pipe axis [31], while this shift becomes about 10 mm for the analyzing magnet [32].

We assume that the vacuum chamber is constructed from stainless steel and copper coated on its inner surface. Its aperture is 20 mm.

3.4.2 Analyzing Magnet

Estimation and optimization of the parameters for the analyzing magnet were performed by a series of 2D and 3D computer model calculations [23], [24], [25], [32], [35]. A C-type solid iron core magnet was considered as it facilitates vacuum chamber installation and maintenance as well as simplifies magnetic field measurements. The transverse cross-section of the magnet is presented in Fig. 6 and its main characteristics are listed in Tab. 2.
The magnet iron core is divided into only two parts by a horizontal symmetry plane. This decision gives confidence to realize the tight tolerances for parallelism of the magnet poles and would decrease substantially any field distortions from the joining elements. The coils of the magnet are proposed to be made from 12.5 mm^2 copper conductors with water cooled channels of 7.5 mm diameter. Each pole coil consists of three double pancake coils (4 turns in two layers). The working line of the analyzing magnet is shown in Fig. 7 and the normalized longitudinal B-field integral as a function of the horizontal position (x) in Fig. 8. The curves show the results of field simulations by a 3D computer model for an ideal geometry of the magnet. The magnetic field integral uniformity region extends over $\sim$10 mm for the anticipated beam energies, as indicated by the box with 20 ppm relative uncertainty limits. However, due to manufacturing errors expected the common uniformity region might be reduced to about 5 mm, which is still

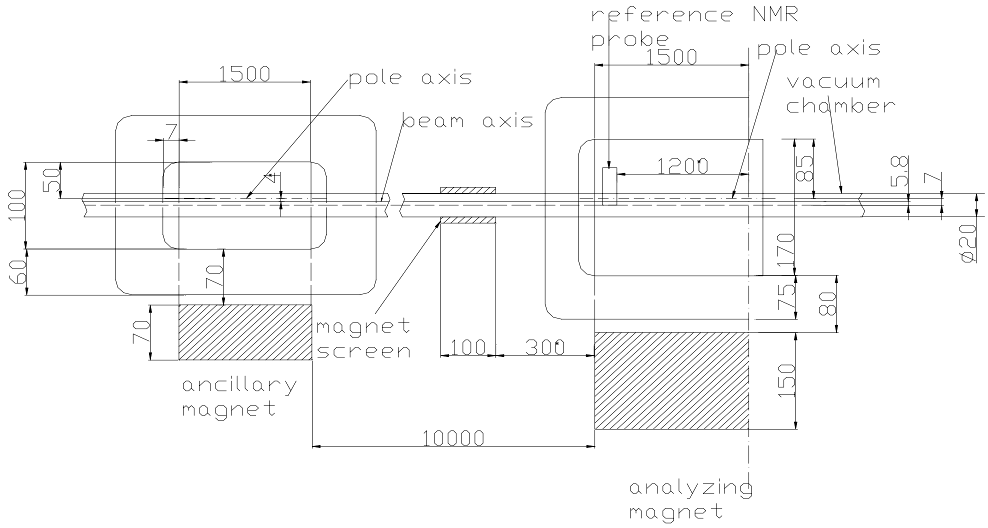

Figure 5: Principal drawing of half of the spectrometer magnet system (plan view).

sufficient for spectrometer working procedures.

3.4.3 Ancillary Magnets

Each of the ancillary magnet should provide a beam bend of 0.5 mrad with opposite signs. The exact value of this angle has, however, to be adjusted by the beam position required at the exit of the spectrometer. This implies no necessity to measure the magnetic field integrals of the ancillary magnets with high accuracy. The less stringent requirements on the ancillary magnets lead to some simpler mechanical design. Also, a C-type solid iron core magnet is considered. The procedure for estimation and optimization of the ancillary magnet parameters is described in [27], [30], [31], [35]. The transverse cross-section of the magnet is shown in Fig. 9 and Tab. 3 presents the basic parameters.

The iron core of the magnet is proposed to consist of five parts (2 poles, 2 horizontal yokes and 1 vertical yoke). The coils should be made of 8.5 mm^2 copper conductors with water cooled channels of 5.3 mm diameter. Each pole coil consists of three double pancake coils (5 turns in two layers). The working line of the ancillary magnet is presented in Fig. 10, while Fig. 11 shows the normalized longitudinal magnetic field integral against the horizontal position. The field integral uniformity region with a precision of $2 \cdot 10^{-5}$ or better extends over some 7 mm for beam energies between 45 and 400 GeV. The spectrometer performance does not suffer from this relatively small uniformity range as the final field strength in these magnets has to be adjusted for an optimized beam position at the spectrometer exit.

3.4.4 Magnet Tolerances

For the analyzing magnet the most critical tolerance issue for its manufacturing and field achievement is the pole gap. Magnet tolerances were estimated by computer models as described in [26], [29]. If, for example, the pole gap varies by 40 μm, the common uniformity region of the magnetic field integral (Fig. 8) will decrease from 10 to 7 mm and its transverse position shifts by 20 mm from the predicted one. Shifts of the uniformity region can be detected during the magnetic field measurement campaign and corrected for when the final position of the magnets

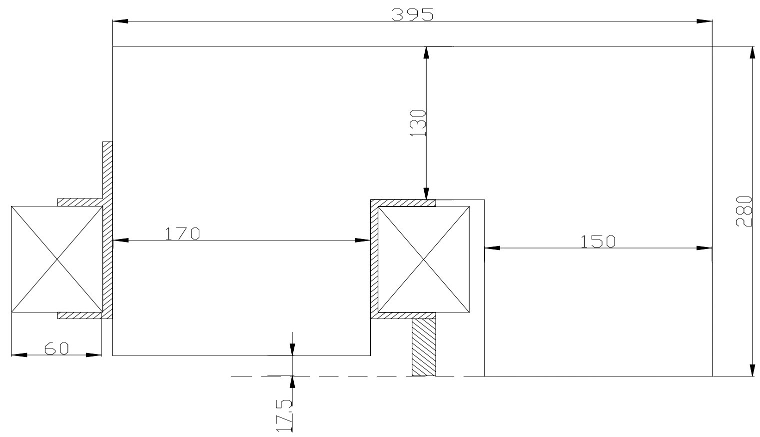

Figure 6: Cross-section of the analyzing magnet (1/2 part).

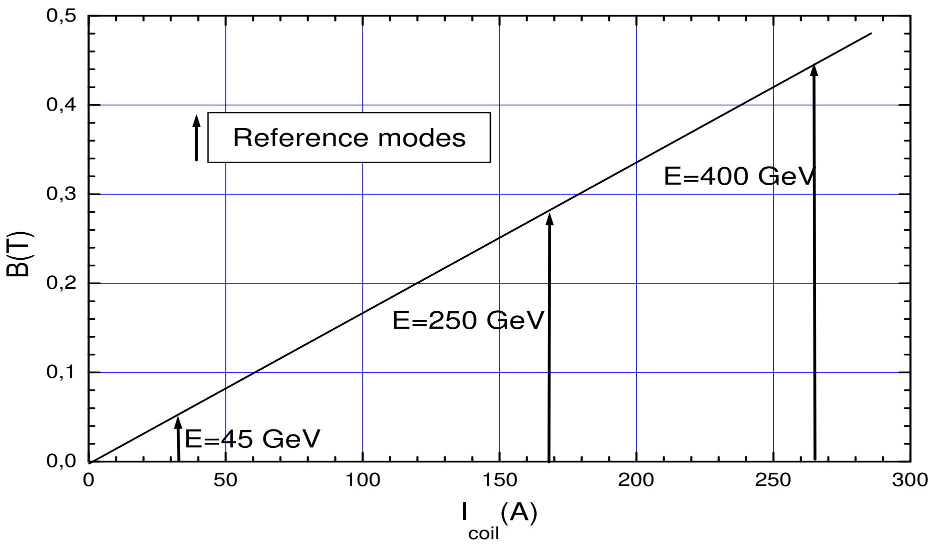

Figure 7: Working line of the analyzing magnet.

in the beamline is known. A summary of basic tolerances for both types of magnets is presented in Tab. 4.

The demands for the materials of the analyzing magnet (Tab. 5) ensure relative variations of the longitudinal field integral of no more than 20 ppm. The impact of the vacuum pipe with some material requirements as shown in Tab. 6 result to a 60 ppm field uncertainty. This requires the necessity of magnetic field measurements inside the beam pipe. NMR probes inserted into the pipe need free space of at least 19 mm in diameter.

The use of magnet end-field screenings reduces the uncertainty of the magnetic field integral substantially. For fringe fields smaller than 0.1 mT as anticipated in our design and utilizing identical screenings along both spectrometer lever arms results to a field integral error of less than 12 ppm.

Position tolerances for the analyzing and ancillary magnets are given in Tab. 7, while the magnet coordinate system used is shown in Fig. 12.

	Analyzing magnet
Magnetic field (min/max)(T)	0.05/0.44
Pole gap (mm)	35
Yoke type	C
Yoke dimensions (mm)	395x560x3000
Yoke weight (t)	4.51
A*turns (1 coil)(max)	6335
Number of turns (1 coil)	6*4=24
Conductor type, sizes (mm)	Cu, 12.5x12.5, ⊘7.5
Conductor weight (t)	0.36
Coil current (max)(A)	264
Current density (max)(A/mm^2)	2.4
Coil voltage (max)(V)	13.3
Coils power dissipation (max)(kW)	3.5
Number of water cooling loops	6
Length of cooling loop (m)	56
Water input pressure (Bar)	6
Water input temperature (deg C)	30
Maximal temperature rise of the cooling water (deg C)	1.4

Table 2: Basic technical parameters of the analyzing magnet.

3.4.5 Magnet Temperature Stabilization

The temperature stabilization of the analyzing magnet is discussed in [26]. Changes of the temperature of the spectrometer magnet lead to variations of the magnet's transverse geometry, particularly of their gaps, variations of the longitudinal geometry of the magnets (particularly of their pole lengths) and variations of the iron permeability. Resulting temperature factors for two magnetic field values (0.05 T and 0.44 T) are collected in Tab. 8.

In order to stabilize the temperature of the analyzing magnet we propose to account for

- a temperature stabilization cooling water circuit with an accuracy of better than 0.2^{o}C;
- monitoring of selected magnetic field points by NMR probes at least in two positions;
- monitoring of the magnetic field integral by the moving wire technique;
- monitoring of the temperature of the magnetic iron core and current coils utilizing sensors with a sensitivity of 0.05^{o}C.

3.4.6 Magnet Hysteresis and Zero-Field Adjustment

For iron core magnets hysteresis effects require special procedures to achieve B-field integral reproducibility. For example, the LEP magnet spectrometer excitation procedure including degaussing and ramping cycles, bending modulation, temperature control and field control by NMR probes in four points achieved a field integral reproducibility with a precision of 15 ppm. The problem of zero-field adjustment can be solved by degaussing cycle procedures if controlled by e.g. special vibrating wire measurement techniques [36].

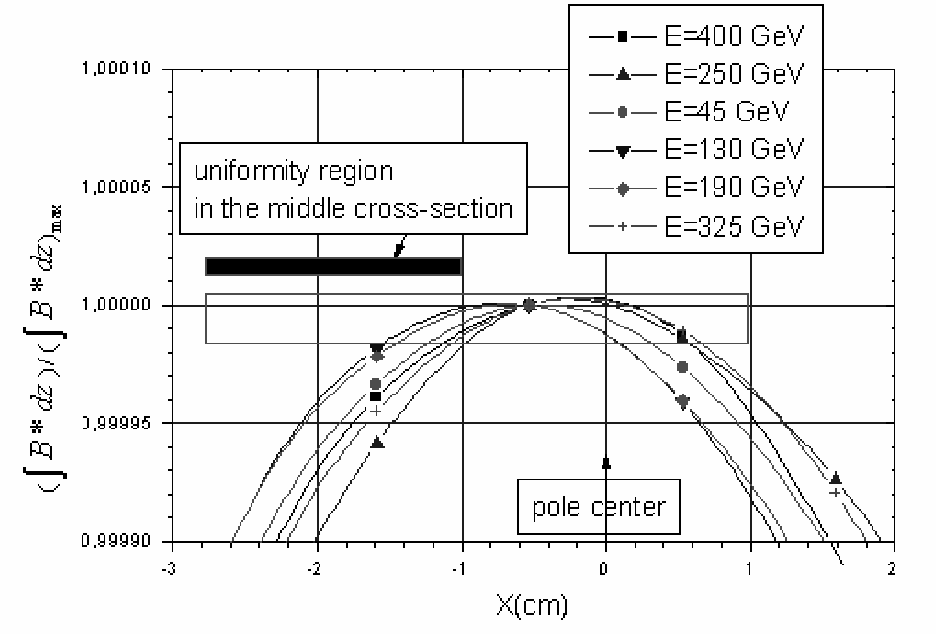

Figure 8: Normalized longitudinal magnetic field integral versus horizontal position. The 20 ppm relative uncertainty range of the field integral is also indicated.

3.4.7 Magnet Power Supplies

For the magnet coil excitation the use of two power supplies are proposed. One should be used for the analyzing magnet and one for the two ancillary magnets, connected in series. The power supply requirements are listed in Tab. 9. The power supplies are standard devices and do not demand additional R&D effort. Stabilization of the magnetic field integral will be achieved by dedicated power measurement and control procedures.

3.4.8 Cooling System

The parameters of the cooling water circuit are of major importance for the temperature stability of the magnets. The temperature should be measured at the entrance and exit of the analyzing magnet. Temperature probes inserted in the core of the magnet are also very helpful. A control regulation scheme maintains the core temperature as constant as possible. For example, stabilization of the water temperature at the entrance of the magnet at a level of at least 0.2^{o}C would result to a variation of the field integral smaller than 10 ppm. A temperature regulation system as realized at LEP would achieve an accuracy as demanded and might be directly used for our purpose.

3.4.9 Control System

The magnet control system should be an integrated part of the energy spectrometer control system. The system for the magnets has to account for

- power supply control;
- control of analyzing magnetic field measurements in at least two points by the NMR teslameter;

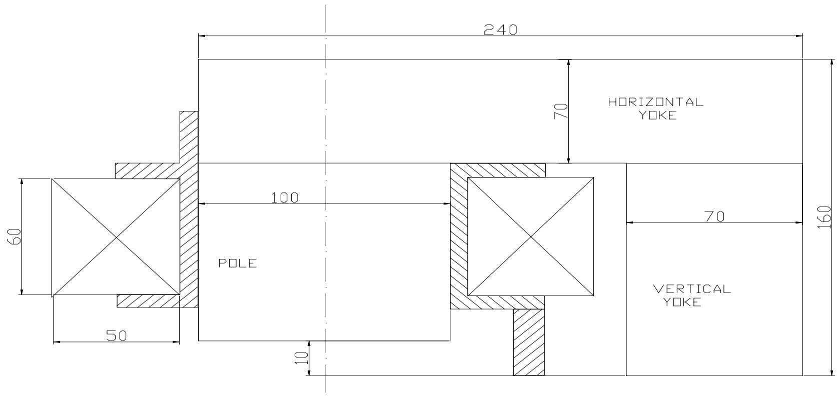

Figure 9: Cross-section of the ancillary magnet (1/2 part).

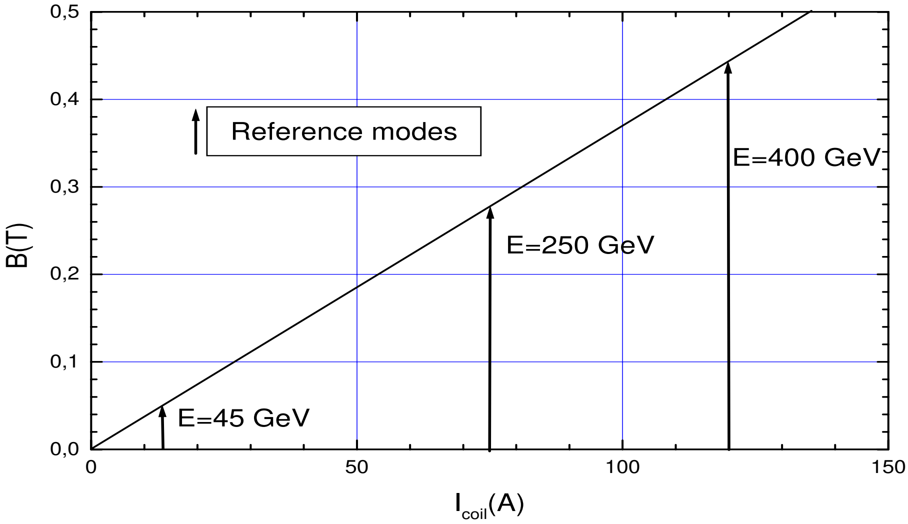

Figure 10: Working line of the ancillary magnet.

- control of analyzing magnetic field integral measurements utilizing the moving wire measurement technique;
- control of the zero-field status of the analyzing magnet utilizing the vibration wire measurement technique;
- monitoring the analyzing magnet iron core and its temperature by about 30 temperature sensors;
- and cooling water stabilization scheme.

Details of the control system of the spectrometer can be found in Sect. 3.6.3.

3.4.10 Synchrotron Radiation Light

Basic properties of the synchrotron radiation (SR) light from the spectrometer magnets are presented in [28]. The power of the SR light determines radiation and heat load of the beam

Magnetic field (min/max)(T)	0.05/0.44
Pole gap (mm)	20
Pole length (mm)	1500
Magnetic field integral (T·m)	0.075/0.665
Magnetic measurement error of the field integral (relative)	(2-5)x10^{-4}
Energy loss due to synchrotron radiation (max)(MeV)	0.01-60
Yoke type	C
Yoke dimensions (mm)	240x320x1500
Yoke weight (t)	0.73
A*turns (1 coil)(max)	3600
Number of turns (1 coil)	$6^{\times}5 = 30$
Conductor type	Cu, 8.5×8.5, $\oslash 5.3$
Conductor weight (t)	0.09
Coil current (max) (A)	120
Current density (max)(A/mm^2)	2.4
Coil voltage (max) (V)	8.5
Coils power dissipation (max)(kW)	1.0
Number of water cooling loops	6
Length of cooling loop (m)	33
Water input pressure (Bar)	6
Water input temperature (deg C)	30
Maximal temperature rise of the cooling water (deg C)	0.7

Table 3: Basic technical parameters of the ancillary magnet.

pipe, surrounding equipment and shielding [6]. It would be desirable to reduce the relative beam energy loss due to SR to a level of $\lesssim 10^{-5}$, which might be achieved e.g. by a three times smaller bending angle or an increase of the length of the spectrometer by a factor of 10. A smaller bending angle however requires a correspondingly improved BPM resolution, whereas a ten times longer spectrometer involves many unpleasant feature and is not recommended at all. Our suggestion is to live with the energy loss and compensate the loss in the measurements.

3.4.11 Magnetic Field Measurements

A review of magnetic field measurement techniques based on experiences at SLAC, CERN and CEBAF is reported in [33]. At these laboratories the following techniques were utilized for precise field determinations:

- moving probes (NMR and Hall);
- moving wires;
- search coils (one or two);
- and flip coils.

[6]SR heat load of the beam pipe and surrounding equipment will be investigated by detailed simulations, with the aim to add possible special arrangement to accomodate the power.

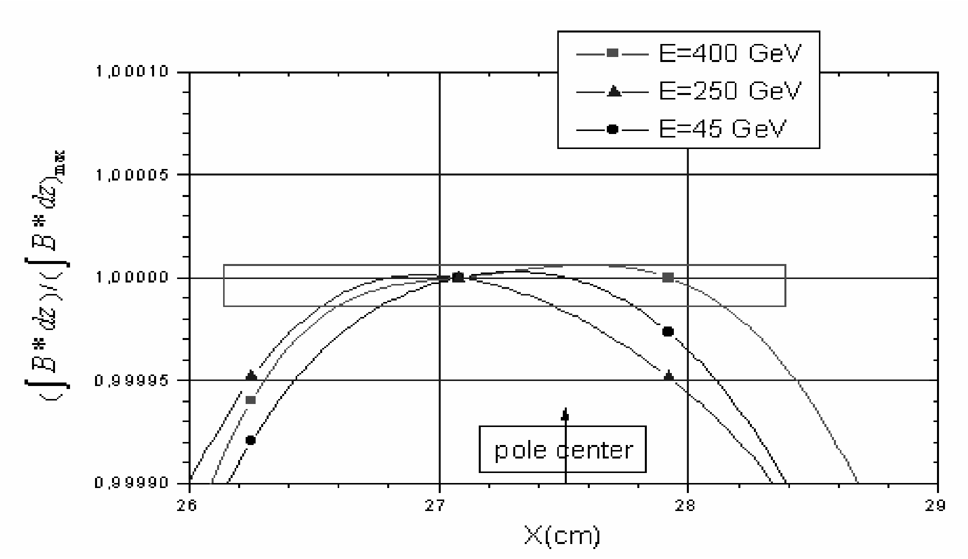

Figure 11: Normalized longitudinal magnetic field integral versus horizontal position. The 20 ppm relative uncertainty range of the field integral is also indicated.

Type of magnet	Analyzing	Ancillary
Poles gap (mm)	0.02	0.1
Pole width (mm)	0.2	0.2
Pole length (mm)	0.5	0.5
Coils vertical position (mm)	1	1
Coils horizontal position	1	1

Table 4: Basic magnet manufacturing tolerances.

Designed and practically achieved relative tolerances for the magnetic field integral are within 10-100 ppm, as shown in Tab. 1. For the energy spectrometer at the future LC, the technique with best precision for local field and field integral determinations should be chosen.

3.4.11.1 Laboratory Field Measurements

It is proposed to apply two independent techniques for field measurements in the laboratory:

- moving probes: NMR probes in the main field region and Hall probes in the fringe field regions;
- two search coils as used at CEBAF.

Moving probes allow for absolute magnetic field determinations. This technique measures the field integral by driving a NMR respectively Hall probe along the length of the magnet in small steps. The probes are mounted on a support device (rigid rod) which can be moved in two directions, either along the beam (z-) direction or in transverse direction. For precise probe positioning in longitudinal direction a laser interferometer should be utilized, whereas a linear encoder with less accuracy is sufficient in transverse direction. A detailed description of the proposed field measurement system can be found in [34]. Tab. 10 summarizes expected systematic errors from this technique. The supposed precision of less than 20 ppm for the field integral measurement can be achieved if

Type of magnet	Analyzing	Ancillary
Type of steel (Russia)	St-10	St-10
μ_{max}	~ 3000	~ 3000
Variation of the steel chemical composition (C, Si, Mn) (%)	≤ 5	≤ 10
Cavity defects (mm^3)	≤ 20	≤ 50

Table 5: Basic magnet material requirements.

Type of magnet	Analyzing	Ancillary
Joining elements for magnets parts	Stainless steel for two parts	Usual design
Girder material	stainless steel	Usual steel
Vacuum pipe material	Stainless steel	Stainless steel
μ_r	≤ 1.005	1.01
Wall thickness (mm)	≤ 0.5	1 - 2
End-field screen material	Permalloy	-
μ_{max}	~ 28.000	-
Thickness (mm)	0.5	-

Table 6: Basic requirements for the ancillary magnet elements.

- a NMR measurement system is used in the main magnetic field region;
- the integrated fringe field contribution does not exceed 4% of the total field integral of the analyzing magnet;
- the less precise Hall probe technique is applied in the end-field regions;
- longitudinal distance measurements with high accuracy is performed using a laser system;
- and systematic recalibration of the Hall probes is performed during the mapping procedure.

During repeated measurement of the field maps, readout information is provided from two reference NMR probes, a set of temperature sensors for the magnet core, magnet coil, cooling water of input/output coils and the air in the experimental hall as well as the stabilization device for the power supplies. The control of the whole system can be performed in real time with a PC. Geometrical parameters for the measurement bench and its tolerances required are presented in Tab. 11. Finally, the field integral has to be evaluated from the local field values monitored by properly located NMR reference and Hall probes.

Search coil field integral measuring devices utilize the method of two small coils connected in series and moving them in beam direction. The distance between the centers of the coils should be similar to the nominal length of the magnet. The method, advantageous in many respects, requires that the distance between the centers of the two coils and the central field for each measurement have to be known with an accuracy of 10^{-5}. The first task can be solved during calibration procedures of the coils, while the second needs established NMR probe precisions of better than 5 ppm. The principal measurement scheme is similar to the moving probe technique discussed above. Instead of the Hall Teslameter an integrator with search coils is used and a

Type of magnet	Analyzing	Ancillary
ΔX (mm)	0.5	0.5
ΔY (mm)	0.5	0.5
ΔZ (mm)	0.5	0.5
$\Delta\varphi_{xy}$ (mrad)	1	3
$\Delta\varphi_{xz}$ (mrad)	0.5	0.5
$\Delta\varphi_{yz}$ (mrad)	0.3	0.3

Table 7: Tolerances for magnet positions within the spectrometer coordinate system.

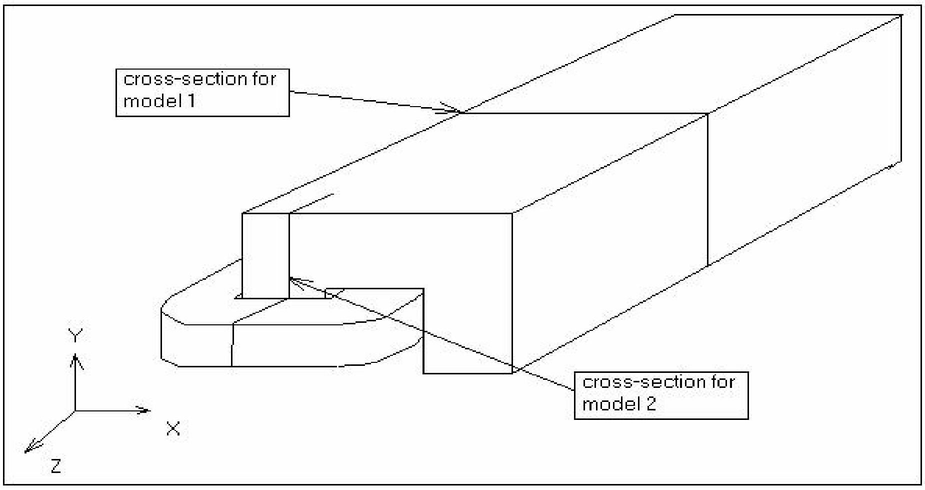

Figure 12: The coordinate system of the magnets.

new mechanical rigid rod for the coils has to be developed. The measurement procedure consists of moving the coils over a distance of about 3 m in a time of few seconds. The control of the longitudinal and transverse coil motion and the readout of the induced voltages are realized in a similar way as for the moving probe method. Two fixed NMR probes are used for magnetic field references and a third one for the readout of the central B-field. Tab. 12 summarizes the systematic errors expected from this technique. A total uncertainty of 14 ppm seems to be attainable.

3.4.11.2 Magnetic Field Measurements in Situ

Basically, field measurements in situ are proposed to rely on two independent techniques:

- reference NMR probes at two fixed predetermined points
- and the moving wire technique for field integral determination.

After finishing the field measurements in the laboratory, the magnets installed into the LC beamline need some final test measurements. Field measurements inside the beam pipe should be performed using the probe techniques (NMR and Hall probes) with specially designed probe holders. For this purpose, a large part of the equipment developed for the search coil technique can be utilized. During the measurements final calibration of the two properly located reference NMR probes should also be performed. Field integral values are then evaluated by accounting

Analyzing magnet field (T)	0.05	0.44
Magnet steel (10^{-5} $1/^{o}$C)	1.24	1.24
Transverse (10^{-5} $1/^{o}$C)	-1.36	-1.3
Longitudinal (10^{-5} $1/^{o}$C)	1.24	1.24
Steel permeability (max) ($1/^{o}$C)	10	10
Permeability (10^{-5} $1/^{o}$C)	5.7	5
Summary (10^{-5} $1/^{o}$C)	5.6	4.9

Table 8: Impact of temperature changes to the analyzing magnet.

	Analyzing	Ancillary
Nominal current range (A)	30/265	13/120
Maximal current (A)	300	150
Nominal voltage range (V)	1.4/13.3	2×(0.9/8.5)
Maximal voltage (V)	15.1	2×10.6
Nominal power (kW)	0.04/3.5	2×(0.01/1)
Maximal power	4.5	2×1.6
Long term current stability (ppm)	10	10

Table 9: Parameters of the power supplies. Effects due to the length of connection conductors are not taken into account.

for the local fields monitored by the probes, the field maps from the laboratory measurement campaign and the final test measuremets.

The magnetic field integral reproducibility depends on the magnetic excitation current and the temperature history, which requires history information of the reference probe locations. At LEP for example, relative field integral reproducibility of 15-20 ppm has been achieved by using the reference NMR probe technique.

Also, the **moving wire** technique is appropriate to perform accurate integrated field measurements. Here, a wire is passed through the gap of the magnet and returns outside to form a closed loop. Transverse motions of the wire in the magnetic field induce a voltage in the loop. Precise measurement of the voltage integral and the distance moved allow to evaluate the integral of the magnetic field. Calibration of this method is achieved during the laboratory measurement campaign by means of absolute moving probe measurement techniques. The scheme of the measurement is in many respects the same as that for the search coil method. Transverse wire motion devices should however replace longitudinal moving techniques. Possible error sources expected are collected in Tab. 13, resulting to a total systematic uncertainty of 19 ppm, a number as anticipated.

A possible arrangement for the NMR and Hall probes and the moving wire technique within the analyzing magnet is shown in Fig. 13.

The precise determination of the absolute beam energy as demanded by physics requires the knowledge of any residual fields from e.g. additional magnets in the beamline and other ambient fields, including the Earth's field, on the beam axis in the inter-magnets sections. The ambient field has been carefully considered and, if necessary, partially shielded, partially included in the integral measurement and partially corrected. Its reproducibility must be checked periodically, since this type of field depends on the history of activities in the tunnel and will therefore vary over time.

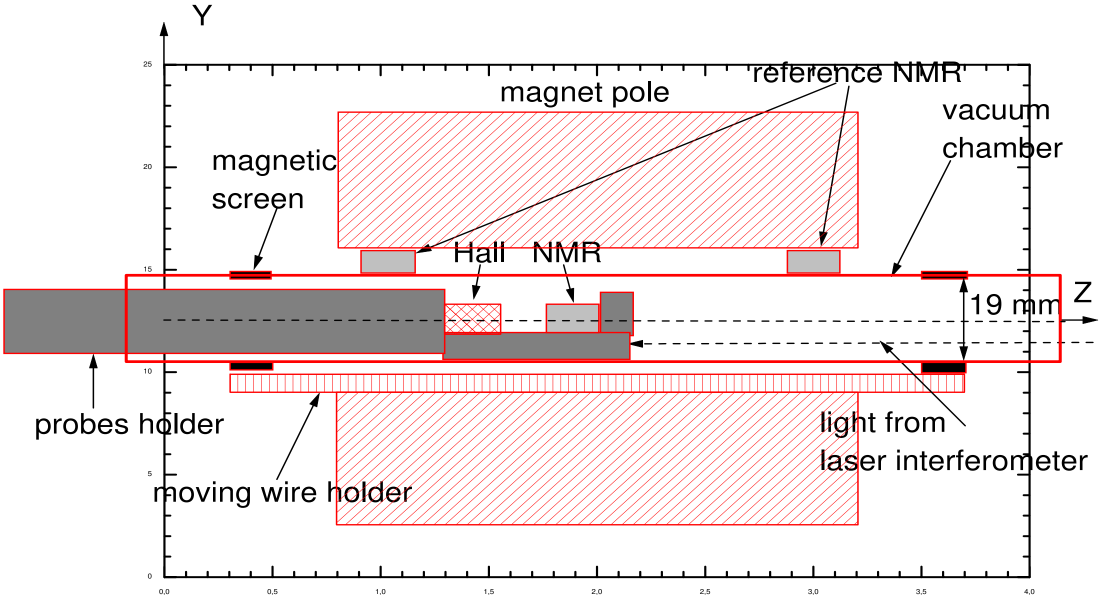

Figure 13: Side view of the probe and moving wire arrangement (Y-vertical direction, Z-beam direction) for in situ measurements inside the vacuum pipe.

Error Source	Error (ppm)
Position determination (laser)	1
Misalignment of laser to beam path	0
NMR system	5
Hall probe precision (100ppmx4%)	4
Hall probe tilt	2
Linear interpolation	8
Total systematic error	20

Table 10: Systematic errors for the moving probe method.

For the small-angle 0.1 mrad spectrometer option, the magnetic field integral has to be lowered by a factor of 10. This can be achieved by reducing the length of the analyzing magnet[7] to 2 m and the strength of the B-field to 0.0075-0.066 T (for E_b = 45-400 GeV). First technical parameters of the current coil needed are reviewed in [37]. Precise measurements of the field integral can be achieved by utilizing NMR and Hall probes, search coil and moving wire techniques.

3.4.12 Ancillary Measurements

In order to provide very accurate field measurements additional calibration and measurement effort is required. In particular, calibration of the Hall probes with periodical recalibrations and of the search coils are of great importance.

During commissioning of the measurement stand in the laboratory the following tasks are mandatory:

[7]The magnet type for this option should be again a magnet with warm current coil and an iron-less core.

Longitudinal region	3800 mm	Step size of measurement
Common region for Hall and NMR probes	2920 mm	10 mm
Region for Hall probe	2*440 mm	5 mm
Position tolerance for the probe in beam direction	1 ppm	
Transverse region	10 mm	1 mm
Position tolerance for the probe in transverse direction	0.1 mm	
Transverse offset of the measurement region from the magnet pole axis (ΔX_{mm}) / its possible adjustment	5 mm/$\pm$5 mm	

Table 11: Geometrical data set for the moving probe measurement bench.

Error Source	Error (ppm)
Position determination (laser)	1
NMR probe	5
Distance between coils axis	7
Integration of the coils output signal (100 ppm * 1%)	1
Total systematic error	14

Table 12: Systematic errors of the search coil method.

- tests of the mechanical equipment tolerances;
- tests of the laser interferometer;
- positioning and alignment tests for the NMR and Hall probes and the coils.

Additional effort is also needed to perform field measurements inside the vacuum chamber of 20 mm diameter. Special measurements are required to provide convincing reliability of the results. Furthermore, some investigations are needed to fix e.g. possible magnetic effects from special screens (μ-metal jackets around the beam pipe) at the end points of the analyzing magnet.

3.5 The Beam Position Monitors

3.5.1 Introduction

The requirements on the beam position monitor (BPM) system for the proposed energy spectrometer are very stringent. In particular, transverse beam position measurements of nanometer range accuracy with excellent stability, large dynamic range, time resolution enabling bunch-by-bunch measurements and a simple mechanical design with micrometer production tolerances are needed.

In order to meet these requirements it was decided that radio frequency (RF) cavity BPMs were the best choice. A pair of cavities resonant at 5.5 GHz was designed in a monolithic block. The high-resolution cavity uses a novel scheme of the dipole mode coupling that in principle has

Error Source	Error (ppm)
Distance determination (laser)	1
Misalignment of travel	8
Digital integrator accuracy (with calibration by moving probes)	10
Total systematic error	19

Table 13: Systematic errors of the moving wire method.

zero coupling to the monopole modes. The other cavity, the reference cavity, operates at the monopole mode and is used to determine the phase, the bunch charge and serves as an local oscillator (LO) signal source.

Before the production of the first prototype comprehensive simulations of the monitor were performed. The results obtained and subsequent tests will be presented and discussed in the following sections.

3.5.2 Cavity BPM Basics

A bunch traveling along the cavity axis with some offset from its center excites the eigenmodes of the cavity, in particular the monopole modes TM_{010}, TM_{020} and the dipole mode TM_{110}. The strongest excitation has the mode TM_{010} (Fig. 14), with largest normalized shunt impedance R/Q. This mode is insensitive to the beam offset and depends essentially on the bunch charge.

The mode of interest is the dipole mode TM_{110}, which is sensitive to the beam displacement and the bunch charge. If the sign of the offset changes, the phase of the dipole mode jumps by 180^0, so that its direction can be detected by means of a beam-locked phase reference.

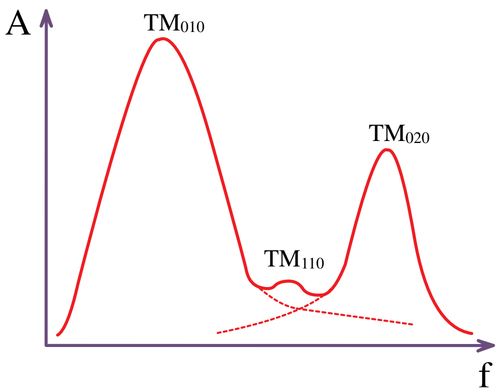

Figure 14: Cavity excitation spectrum as a function of frequency

If a bunch of particles with some charge q passes through the cavity the excitation of the TM_{110}-mode has a linear behavior in the beam-pipe region, so that the output voltage is given by [38]

$$V_{out} = \frac{\omega}{2}\sqrt{\frac{Z}{Q_{ext}}\left(\frac{R}{Q}\right)_f} q \frac{x}{x_f}, \tag{5}$$

where Q_{ext} is the external quality factor, characterizing the coupling of the dipole mode signal, ω the frequency, $(\frac{R}{Q})_f$ is the normalized shunt impedance of the cavity for a given offset x_f and

Z is the impedance of the extraction line. This implies that the TM_{110} peak signal does not depend on the material of the cavity but only on its geometry.

The time resolution of the monitor depends on the loaded Q-factor, which involves both the external and internal quality factors Q_{ext} and Q as

$$\frac{1}{Q_L} = \frac{1}{Q} + \frac{1}{Q_{ext}} \tag{6}$$

and therefore accounts for the power dissipated in the cavity walls and the output power. The energy stored in the cavity decays exponentially with the time constant $\tau = \frac{Q_L}{\omega}$ when the bunch has left the cavity. To ensure bunch-by-bunch measurements, this energy has to be negligible before the next bunch excitation occurs. The highest acceptable Q_L for a given decay $D = \frac{V_{rest}}{V_{out}}$ at the bunch distance t_b is known as [38]

$$Q_L = \frac{\omega t_b}{2 \ln D}. \tag{7}$$

Q_L can be varied by changing the cavity material and/or the coupling strength.

3.5.3 The Beam Induced Signal

The beam induced signal of a cavity RF BPM contains several components, the offset signal and some background signals that limit its resolution and precision[39]:

$$V_{110} = V_{110}(x) + V_{010} + V_{110}(x') + V_{110}^{\perp} + V_{noise}. \tag{8}$$

The first term is the offset dependent dipole mode signal, as given by eq. (5).

The V_{010} component represents the leakage of the monopole mode signals at the dipole mode frequency, see Fig. 14. In general, only the first two monopole modes influence the measurement because of their high R/Q values. The signal caused by these modes is usually much stronger than the dipole mode signal and deteriorates even for small leakage the BPM accuracy. Also, saturation of the signal processing electronics might occur. In order to avoid such negative impacts of the monopole modes, they have to be damped. Basically, some mode-selective solution is needed to achieve this requirement.

The component $V_{110}(x')$ represents the dipole mode signal caused by a bunch with non-zero inclination angle with respect to the cavity axis. For small angles $x' \lesssim$ few mrad this component relative to the beam-position signal can be estimated as

$$\frac{V_{110}(x')}{V_{110}(x)} \simeq \frac{i}{k} \frac{x'}{x} \Big(1 - \frac{kl}{2} \cot \frac{kl}{2}\Big), \tag{9}$$

where l is the monitor length and k is related to the wavelength λ, $k = 2\pi/\lambda$. The beam-angle signal exists even for centered beams and can be comparable to or even larger than the offset dependent dipole mode response. It is essential for high-precision cavity monitors to keep this signal on a negligible level. It has to be minimized by optimization of cavity parameters. The ratio $\frac{V_{110}(x')}{V_{110}(x)}$ decreases with increasing TM_{110} frequency, on the costs of more complicated signal processing electronics and tighter mechanical tolerances of the BPM.

The term $V_{110}^{\perp}$ in eq.(8) is caused by the interaction of the orthogonal polarizations of the dipole mode, the so-called cross-talk. For the monitor proposed here the horizontal beam displacement will be measured. Therefore, only one polarization is coupled out and the impact of the other is automatically removed.

The thermal noise produced by the BPM, V_{noise}, is estimated as

$$V_{noise} = \sqrt{4kTZ\Delta f}, \tag{10}$$

where $k = 1.38 \cdot 10^{-23}$ W·s/K is the Boltzmann constant, T the temperature of the BPM (in Kelvin), Z the impedance of the extraction line and Δf the bandwidth of the monitor (usually the 3 dB-range of the dipole mode resonance curve $\Delta f = f_{110}/Q_{110}$ is taken for its estimation). If eq.(10) is multiplied with the noise factor of the electronics, the full noise of the BPM system is obtained.

From this discussion important demands for nanometer resolution cavity BPMs can be derived: a large TM_{110} displacement signal, efficient rejection of the monopole mode leakage, negligible beam-angle signal and low-noise BPM and electronics.

3.5.4 Monitor Design

A simple cylindrical pill-box cavity with a novel slotted structure has been proposed to meet the demands. For the coupling of the horizontal polarization of the dipole mode, two rectangular waveguides arranged in vertical direction are used. Fig. 15 shows a sketch of the system. The slots couple the dipole mode in the cavity to the TE_{10}-wave in the waveguides (Fig. 16). At the same time, the monopole modes couple to the higher TE_{11}-wave in the waveguides, which has a higher cut-off frequency. Since the height of the waveguide is much smaller than its width, the TE_{11}-wave is well below cut-off, while the TE_{10}-wave propagates. In this way a strong rejection of the monopole modes is achieved. Any surviving monopole mode signals are only caused by fabrication errors. Since tolerances for the critical dimensions of the cavity and waveguides can be machined with 1-2 μm precision, monopole mode suppression of more than 100 dB is achievable. Note that the signals in both waveguides have the same phase, monopole mode suppression by means of a 180^0-hybrid is ruled out.

The idea of using a slotted cavity with proper designed waveguides was already mentioned some time ago [40], and similar studies were initiated at other laboratories, see for example [41].

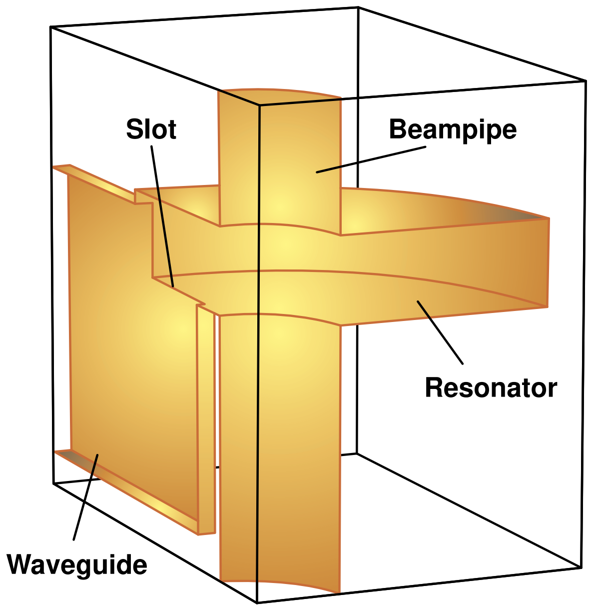

Figure 15: Cavity BPM geometry with coupling slots

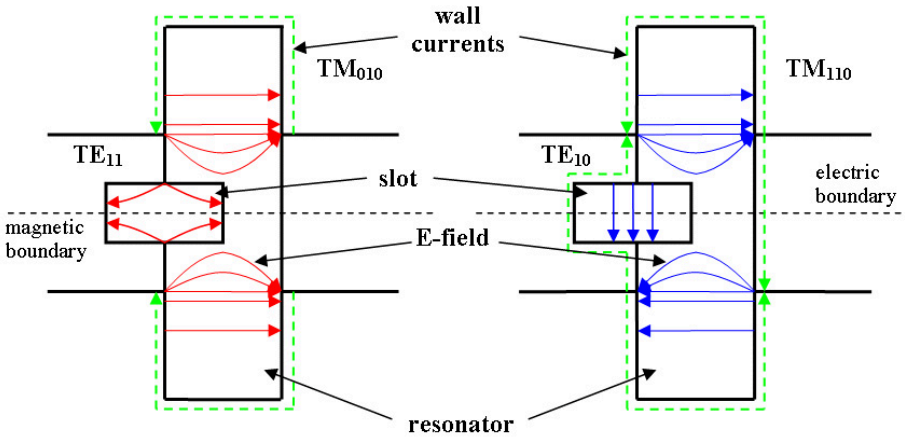

Figure 16: Principle of the coupling scheme using a slotted structure

Important geometrical design parameters of the cavity and the waveguide are summarized in Tab. 14. For illustration purposes, frequency shifts of the dipole mode due to production errors of +100 μm are also given. The most sensitive quantity is the cavity radius. We remind that shifts in the order of 1-2 MHz are anticipated for the BPM.

Dimension	Size, mm	Frequency shift, $MHz/100\mu m$
Radius b	31.40	-13.4
Length l	9	1.04
Beam pipe radius	9	-3.04
Waveguide width	31	-3.85
Waveguide height	4	-7.32

Table 14: Design parameters and frequency shifts of the 5.5 GHz Monitor

The monitor geometry was optimized by means of the computer code GdfidL [42] in order to achieve the highest shunt impedance. Calculated RF-parameters are compared with measured values in Tab. 15. The measurements were performed with an aluminum cavity model using a network analyzer[8]. The dipole mode resonance frequency was supposed to be 5542 MHz, which is very close to the measured value of 5540 MHz despite of a machining error of 10-20 μm. The measured internal Q-values and the correlated damping times are lower than the calculated numbers, mainly because the aluminum model was only screwed together and not welded or brazed. This difference should however not affect resolution measurements, since the output voltage depends on the coupling strength and hence on the external Q-value.

The monopole mode rejection can be estimated by comparison of the ratios of the internal and external voltages produced by the monopole and the dipole mode. Assuming an offset of the coupling slot of 100 μm and a beam offset of 100 nm we get

$$r = \frac{V_{in}^{010}/V_{in}^{110}}{V_{out}^{010}/V_{out}^{110}} = \frac{4460/0.004}{4.3/1.9} \simeq 114 \ dB.$$

This indicates an effective and sufficient monopole mode rejection for a precisely machined BPM.

[8]Except for the numbers in the last row of Tab. 15.

Parameter	Numerical Simulation			Measurement		
	TM010	TM110	Refer.	TM010	TM110	Refer.
f, MHz	3809	5542	5542	3787	5540	5540
Q	2550	2760	1570	580	470	510
Q_{ext}	-	300	320	-	410	300
Q_L	-	270	270	-	220	190
Damping time τ, ns	213	16	16	49	13	11
Bandwidth Δf, MHz	1.5	20.5	20.5	6.5	25.2	29.2
$\left(\frac{R}{Q}\right)$, Ohm	80	0.72 at $x = 1$ mm	17	-	-	-
Int. voltage, V (by $q = 3.2$ nC)	4460	40 at $x = 1$ mm	950	-	-	-
V_{out}, mV (by $q = 3.2$ nC)	4.3/100 μm slot offset	1.9/100 nm beam offset	90	-	-	-

Table 15: Designed and measured parameters of the 5.5 GHz monitor

The bandwidth of the monitor signal determines the minimal bandwidth of the input filter within the signal processing electronics. Using the design value of 20.5 MHz of Tab. 15, the noise leakage is estimated to about 4 μV, and a sensitivity of 1.9 mV/100 nm can be expected for a linear collider bunch charge of 3.2 nC. This means that a position resolution of few nanometers is theoretically possible. The limiting factor of the resolution is the beam-angle signal, which is expected to be as strong as a 400 nm beam offset TM_{110} signal. The beam-angle signal can be reduced by e.g. a factor of 4, if the length of the cavity is two times smaller. It is in principle also possible to take into account the 90 degree phase difference between the beam-angle and the offset signals within the electronics to eliminate this noise signal.

Besides the position monitor, a reference cavity with the TM_{010} mode frequency of 5542 MHz, the dipole mode frequency of the monitor, was designed to provide

- the phase reference
- the LO-signal for the read-out electronics
- the bunch charge.

This cavity has a diameter of 46 mm and is 4 mm long. The signal is coupled out by only one waveguide similar to those of the position cavity. It is however rotated by 90^0 with respect to the position monitor waveguides in order to couple to the monopole mode.

The components of both cavities and the waveguides were machined out of a single aluminum block. The position cavity and its waveguides were machined at one end and the reference cavity at the other end (Fig. 17). Both cavities are closed by 1 cm thick plates. The coaxial adapters are realized with UHV feedthroughs from KYOCERA with an output impedance of 50 Ω. The inner connector has contact to the opposite waveguide wall, so that magnetic coupling is realized. Gold-plated sockets from HARWIN were used to provide good electrical contact.

3.5.5 Read-Out Electronics

The signal detection scheme is based on a homodyne receiver (Fig. 18). Basically, the input signal is down-converted by means of a local oscillator (LO) signal with the same frequency into

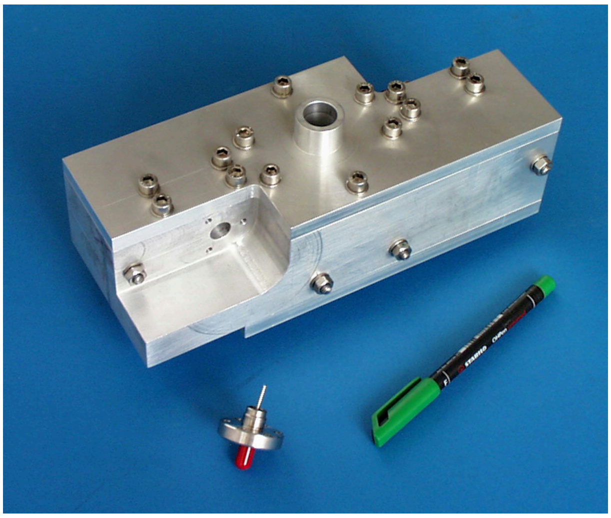

a) Prototype assembled

b) Position cavity disassembled

c) Reference cavity disassembled

Figure 17: 5.5 GHz monitor prototype

the direct current. The amplitude and the polarity of the down-converted signal are proportional to the initial BPM signal.

The input signals from both cavities are first filtered by a band pass filter (BPF) having a center frequency of 5542 MHz and a bandwidth of about 200 MHz to suppress unwanted harmonics and reduce the noise[9]. Then, the position signal is splitted by a power divider into two signals for the I/Q mixer and down-converted using the LO-signal delivered from the reference cavity. The I/Q mixer provides two signals, one in phase (I) and one in quadrature (Q), i.e. shifted by 90^0. Synchronization of the detection system is adjusted with a phase shifter. The down-converted signals are amplified and delivered to the analog-to-digital converter (ADC). In this way, amplitude and phase of the offset signal are calculable as $S = \sqrt{V_I^2 + V_Q^2}$ and $\phi = \arctan \frac{V_Q}{V_I}$. The reference signal also serves for the bunch charge measurement. Possible components of the electronics are summarized in Tab. 16.

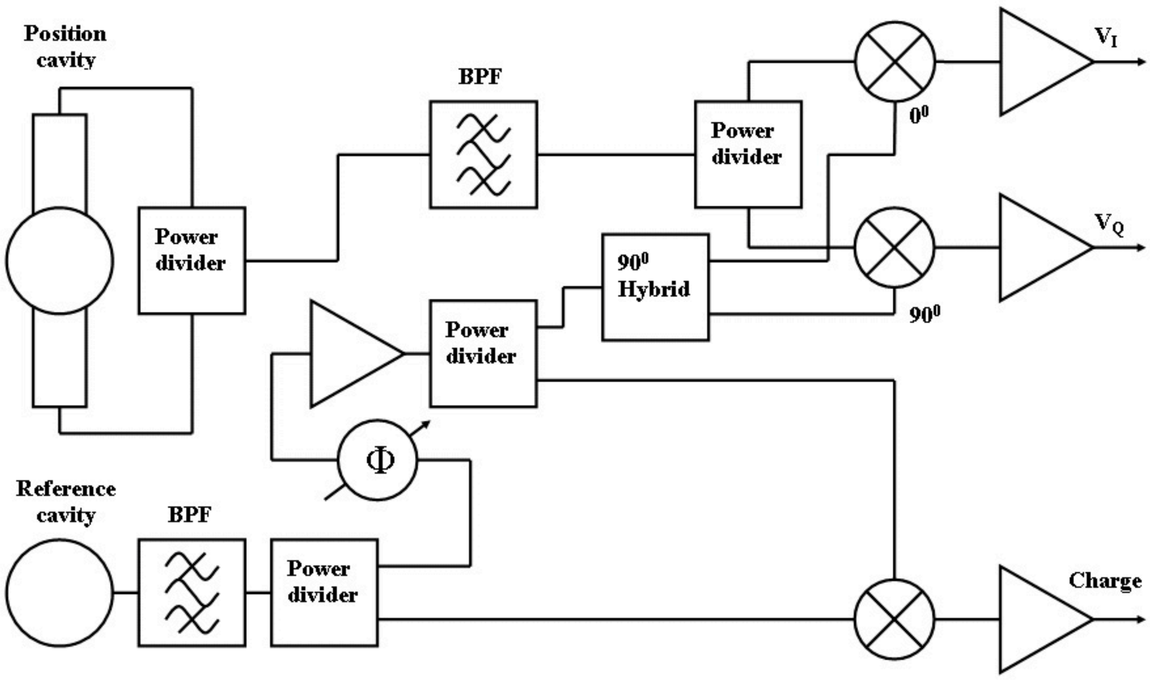

Figure 18: Block-scheme of the read-out electronics for the 5.5 GHz monitor

The most important parameters characterizing the receiver circuit are the dynamic range, signal losses and the noise factor. The noise factor defines the minimal signal level which can be processed. It is therefore directly related to the resolution of the monitor. Losses in the electronics have to be minimized to avoid a small signal-to-noise ratio. The dynamic range of the receiver depends on the noise and the maximal signal level, which can be accepted by the components without saturation. The proposed processing scheme covers actually a dynamic range of about 80 dB, which corresponds to a maximal beam offset of ±1.3 mm, and a position resolution of about 200 nm. According to the discussion of basic spectrometer parameters in Sect. 3.5.4, it is desirable to increase the linearity of the BPM electronics to at least ±2.5 mm, which, however, requires an improved dynamic range of the I/Q mixer with a higher 1 dB-compression point. If this turns out to be not feasible, the non-linear range of the mixers should be used with careful calibration of the electronics. The resolution of the BPM can be further

[9]The optimized bandwidth for the filter is near 30 MHz, but such a filter was not available during the course of this study.

Components	Parameters
Mixers Miteq DM0208LW2	BW 2-18 GHz, LO Power 7-13 dBm Losses 6.5 dB, LO-RF Isolation 30 dB IP3: 15 dBm
Filters	CF 5542 MHz, BW 200 MHz, Losses 3.2 dB
Power Dividers M/A-COM 2089-6208-00 SUHNER 4901.19A	BW 2-18 GHz, Balance ±1 dB, Losses 0.6 dB Isolation 20 dB, 1.45 VSWR 6 dB matched divider
Amplifiers RF: Hittite HMC280MS8G IF: AD8001	Gain +18 dB, Max. level +20 dBm f_{max} = 100 MHz, Gain +40 dBm
Hybrid M/A-COM 2032-6371-00	90^0-Hybrid, BW 2-18 GHz

Table 16: Components of the 5.5 GHz-electronics as used for the beam test

improved by using low-loss cables and low-noise signal processing components, in particular low-noise amplifiers and narrow band filters.

Attention should also be paid to the stability of the read-out electronics. In particular, shifts with time should be controlled by an appropriate reference signal introduced by a directional coupler for calibration purposes. The reference signal generator stabilized by a dielectrical resonator has to be an integrated part of the electronics, see e.g. [43].

To maintain the high resolution of the monitor system, a fast 18 bit ADC with appropriate on-board memory should be used for analog-to-digital conversion.

3.5.6 Test Bench and Beam Tests

The aluminum model of the monitor was tested together with the read-out electronics in the laboratory using a test bench (Fig. 19). The beam was simulated by an antenna driven from a signal generator. The antenna could be moved precisely in order to simulate beam offsets. A second antenna was fixed to excite the reference cavity. Signals of the cavities were down-converted with a read-out electronics and digitized.
The dependence of the I and Q output port voltages on the position of the antenna were measured to determine the resolution of the BPM (Fig. 20). A linear fit applied to the measured voltages resulted in a position resolution of about 300 nm r.m.s. for a 100 μm offset range. R.m.s. values for successive increased displacement ranges indicated a dynamic range of the monitor system of about ±0.7 mm, as long as 1 μm position resolution was not exceeded. The resolution and the dynamic range are, however, worse than anticipated, mainly due to the use of broadband components and low-level mixers.

Tests with beam were performed at the accelerator facility ELBE in Rossendorf (Germany). The linac, based on superconducting 1.3 GHz TESLA structures for electron acceleration, provides a maximum beam energy of about 20 MeV and a bunch charge of $\lesssim$ 80 pC.

A copper prototype monitor[10] was installed into a test beamline and accompanied by two

[10]Copper was used for the BPM material to braze the individual monitor components to a common UHV body.

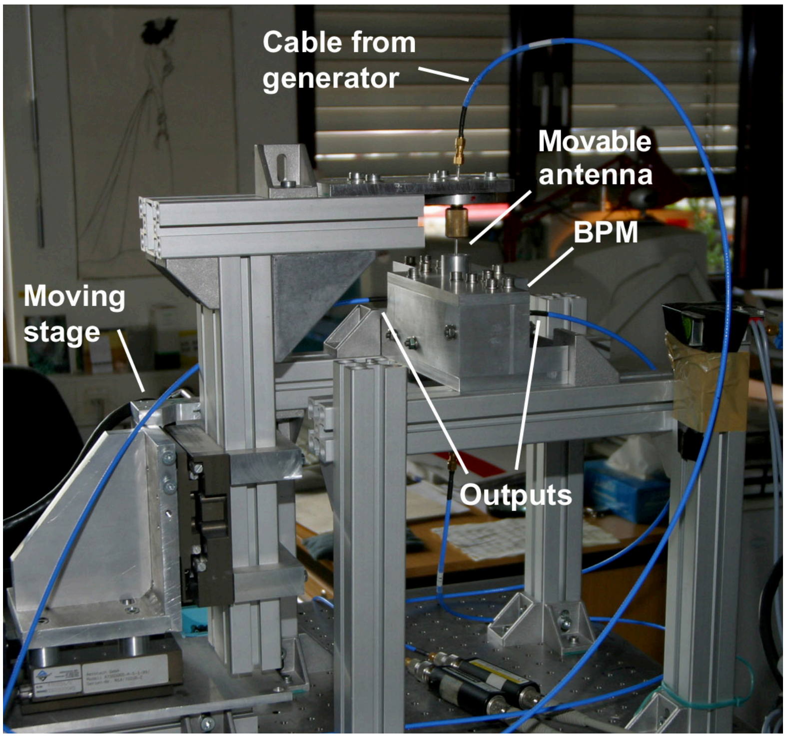

Figure 19: Test bench for the cavity BPM

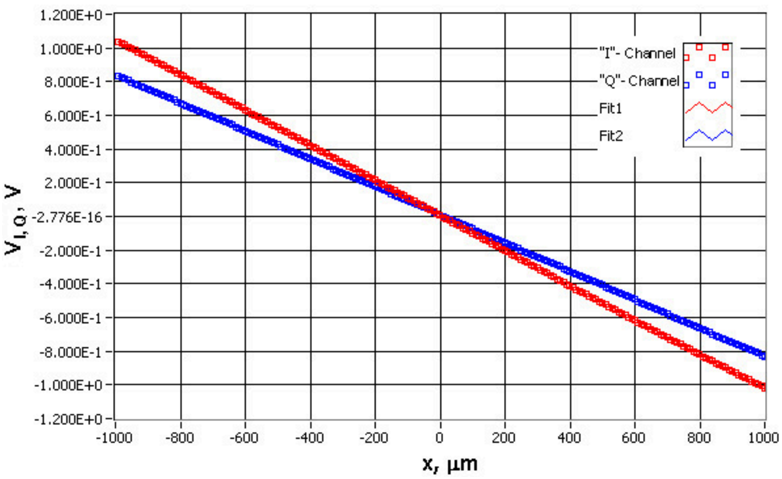

Figure 20: I and Q output voltages against the antenna position

viewscreens to allow for first beam position information (Fig. 21). The beam could be moved transversally with a steerer in a controlled manner, so that relative beam positions in the BPM could be deduced.

At first, measurements of the monitor were performed by means of a spectrum analyzer. The resonant frequency of the dipole mode was found at 5555 MHz. This large value compared to the design TM_{110} frequency is mainly caused by a dimensional error during the fabrication of the BPM. Frequencies in the range of the TM_{010} monopole mode were scanned too, but no signal resonance was observed. This confirms a strong monopole mode rejection of at least 100 dB in the BPM.

Measurements with 300 ns bunch spacing were then performed with the read-out electronics

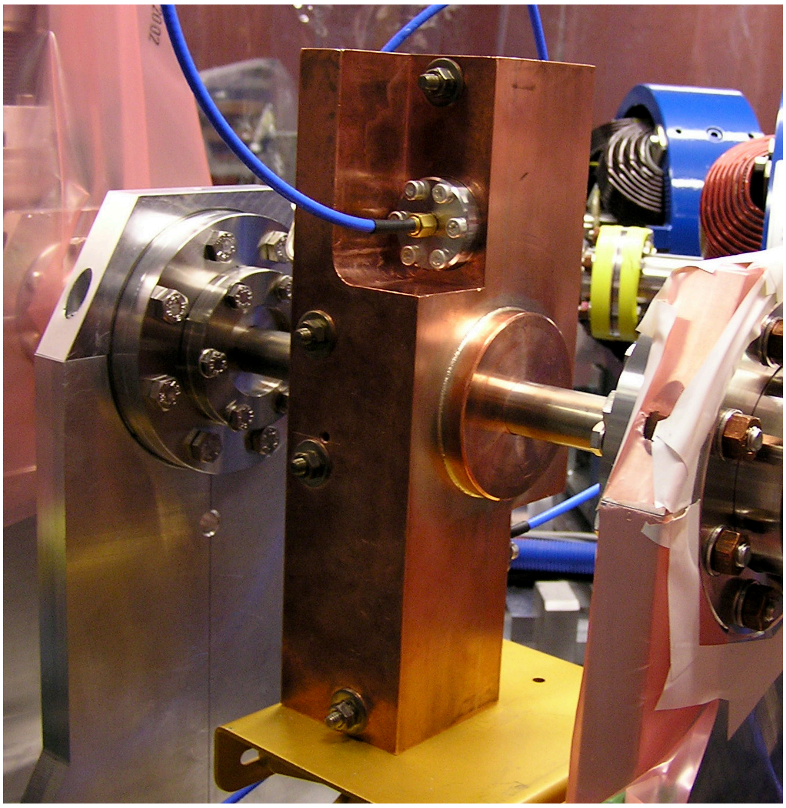

Figure 21: BPM in the test beamline of ELBE

for different beam positions within the monitor. Output signals of the electronics were delivered to a 9-bit oscilloscope, which was utilized for analog-to-digital conversion and to adjust the trigger. For the scope trigger, the beam signal itself was taken provided the peak voltage exceeded a predetermined threshold. A LabVIEW application running on a PC was used to control the scope and transfer the data to a storage disk. Signals were averaged over about 10 bunches to eliminate some possible position and charge fluctuations. Fig. 22 shows the dependence of the I-port voltage against the offset for several bunch charges. A linear dependence of the BPM response on the bunch charge is evident within a very wide offset range. The position uncertainty derived from a linear fit was about 70 μm for a displacement range of $\pm$4 mm and 80 nC bunch charge.

Improved characteristics of the BPM are expected when averaging is performed over about 100 bunches. The charge related information from the reference cavity was taken to normalize the monitor output voltage $V_{out} = \sqrt{V_I^2 + V_Q^2}$, shown in Fig. 23 against the beam offset. It is worth to mention that the LO signal from the reference cavity was too small to be used for down-conversion, although it was amplified. An external oscillator was taken to provide the corresponding signal. From Fig. 23, a position resolution of about 100 μm was derived from a straight line fit over an offset range of $\pm$9 mm. If this value is scaled to the linear collider bunch charge, an accuracy of $\sim$2.5 μm is expected. However, this result should be considered with some caution since, for example, rest beam jitter and possible beam drifts, steerer current uncertainties, large electronic noise, granularity limitation of the intrinsic ADC of the oscilloscope and oversteering of the electronics due to large transverse beam sizes of more than 1 mm preclude any serious position resolution determination.

The time structure of the signals obtained has also been investigated. A damping time of 74

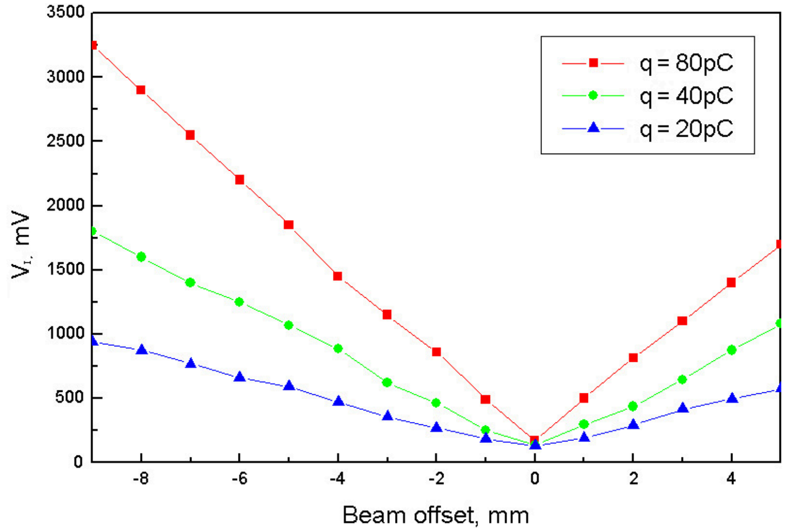

Figure 22: Voltages observed at the I-output port of the electronics

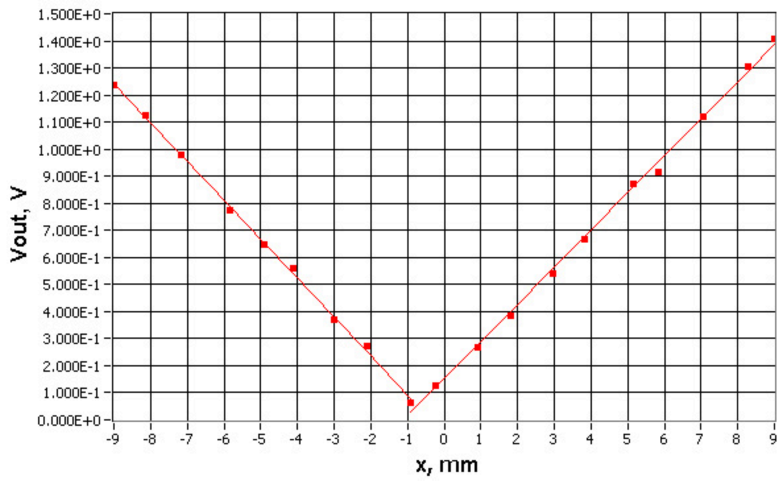

Figure 23: Monitor voltage response on beam displacement with averaging over 100 bunches

ns has been estimated, which should however be improved to about 36 ns in order to ensure a BPM position resolution of 100 nm or better for each bunch. According to the expected small damping times of the monitor (see Tab. 15), time resolution studies of the electronics are needed in the future.

In summary, first tests of a BPM based on a novel slotted cavity with proper designed waveguides indicated functionality as anticipated. In particular, strong monopole mode suppression has been observed. Slight changes of the monitor design could be helpful, but more importantly improvements of the electronics mentioned require further R&D. Beam tests under conditions as close as possible to those expected at a linear collider with 1.3 GHz superconducting RF cavities are needed.

All BPMs and their supports should be temperature stabilized by a cooling circuit. Such a system should provide equal pressure, equal water flow and thus an equal power to all BPM stations. The temperature should be constant within 0.1^oC.

A 1.5 GHz BPM with 80 mm large aperture was also studied in ref. [38]. The principal results support its application for an energy spectrometer based on the TESLA zero-crossing concept and located close to the IP. However, significant effort has to be directed to achieve a position accuracy of $\sim$50 nm, a timing behaviour allowing bunch-by-bunch measurements and strong suppression of the beam-angle signal.

3.6 Stabilization, Alignment and Control of the Spectrometer

For the energy spectrometer with its unprecedented demands on beam energy precision, stabilization, alignment and control are important issues. They have to be carefully considered in the design of the spectrometer, in particular of the BPMs and the magnets. A challenge for the design of alignment and position systems is the rapidly development of their instrumentation and hardware over the last years. Further evolutions are expected in the future, especially during the course of the construction of the spectrometer. Investigating of and following industrial standards is probably a safe path to achieve the goal.

The main effects which influence alignment and positioning of the spectrometer elements are [44]:

- ground motion,
- vibrations
- and thermal expansion

Beam jitter in position and angle, not directly related to stabilization and alignment issues, might also have an impact on the precision of the beam energy determination and is discussed shortly an the end of this section.

3.6.1 Stabilization Issues

Ground motion, vibration and other disturbances can be a limiting factor for the performance of the energy spectrometer. Elimination or at least significant damping of these effects is essential. In the past, several studies of linac performances with respect to ground motion used the so-called ATL [45] model: $< Y >^2 = A \cdot T \cdot L$, where Y is the relative offset of two points separated by a distance L and T is the time since perfect alignment. A is the constant of proportionality, and is generally quoted within the units μm^2 m^{-1} s^{-1}. For the DESY site as an example, a value of $A \approx 4{\cdot}10^{-6} \mu$m^2 m^{-1} s^{-1} has been measured [46], which results to a displacement dispersion of about 50 μm for $L = 2$ m and $T = 2$ weeks.

Ground motion respectively vibration sources are seismic and cultural noise. They can also be produced by the accelerator complex itself. In general, ground motion can be divided into 'fast' and 'slow' motions, with the boundary between them in the region of few Hz. The motion in the low frequency bands is large, on the order of few μm. For frequencies higher than several Hz, the motion is small or even negligible for our case. However, it is important to emphasize that the relative motion of two points separated by some distance is crucial. For reasons of stability and avoiding most ground motion effects between the spectrometer components it is proposed to mount the whole setup on a 25 m long common girder. The girder should be vibration resistant with a low thermal expansion coefficient in order to provide a precise and stable support system. In this respect a new high compressive concrete [47], easily manufactured with performances like natural granite or better, is suggested to be employed and grounded to the floor of the tunnel within the BDS. Such a girder is also sufficient rigid so that it does not amplify ground motion.

Stability issues have to be considered in the design of the mechanical components of the spectrometer. As ground vibration decreases quickly with increasing frequency, the general guideline for the mechanical design of the spectrometer elements is to have a fundamental eigenfrequency as high as possible.

Remaining vibration is most critical for the beam position monitors. Studies to develop active stabilization technologies, see e.g. [48], [49], indicate that vibration amplitudes can be reduced below subnanometer sizes. Also, some form of real-time measurements and compensation of BPM positions might be required. One approach to this problem relies in measuring the positions of the monitors with a laser interferometer and repositioning them with piezoelectric actuators. Recent development of such technology has demonstrated a reduction of vibrations to few nanometers [48]. The required feed-back bandwith is 5-10 Hz, i.e. sampling and control at 10 Hz is adequate, since BPM repositioning within the 1ms long bunch train is (probably) not needed.

3.6.2 Alignment and Position Issues

There are basically two alignment requirements for the spectrometer. The first one concerns the accuracy with which the device as a whole has to be positioned relative to the elements of the beam delivery system. The second demand, which is more stringent, is related to the position accuracy of the spectrometer elements to each other. This aspect is of particular importance for the beam position monitors.

The global alignment system relates the position of the spectrometer within the beam delivery system. It will be a part of the general alignment system of the ILC. An example is discused in ref. [1] by the TESLA collaboration. The proposed intention is to use a system of reference points, which are fixed to the tunnel wall every 20 m to 40 m. Since neither the causeway nor the reference points are suitable to put geodetic instruments on, the instrument will be mounted on a moveable carriage which runs on beams fixed to the tunnel wall above the causeway. The carriage can be fixed to the tunnel wall at certain equidistant positions. The alignment will be carried out with tachymeters, see Fig. 24. A tachymeter does simultaneous measurements of horizontal and vertical angles with an accuracy of 3 μrad and the distance to marked target points with 0.1 mm uncertainty. Such precision is sufficient for the installation of the 25 m long spectrometer support girder within the BDS and for the alignment of the magnets. It is estimated that the standard deviation of every component to be installed is within 0.5 mm horizontally and 0.2 mm vertically over a range of 600 m.

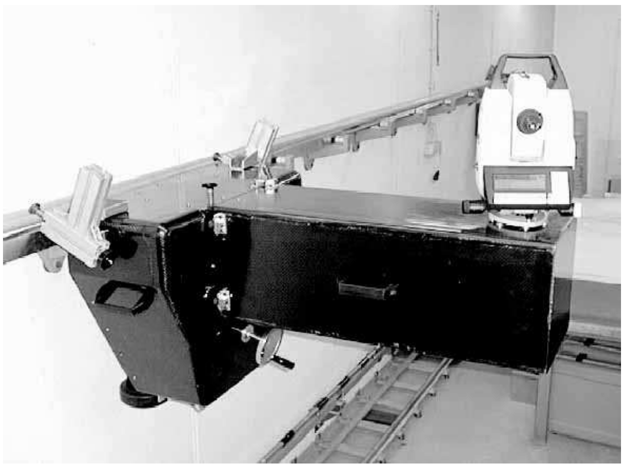

Figure 24: The tachymeter mounted on a carriage.

For initial, coarse location of the spectrometer elements standard moveable elements are foreseen, which support each magnet respectively BPM and are mounted stiff to the common concrete girder. They allow for relative movements of the components to each other with submillimeter accuracy.

Within the spectrometer system, precise alignment of the BPMs with 50-100 μm tolerances in beam direction and 50 nm in transverse direction needs novel approaches. The proposed solution is to apply an optical measurement system using laser straightness monitors and frequency scanning interferometry (FSI) operating in a vacuum tube [50]. It is expected that such a system will overcome the limitations of traditional technologies and can provide an accuracy of $\mathcal{O}(1\mu\text{m})$ over a distance up to 25 m. By combining the FSI measurement with Michelson interferometry (M-FSI) it is feasible to obtain a sensitivity to transverse offsets of nanometer-scale size. This makes the M-FSI system suitable for BPM transverse alignment with uncertainties of 50 nm or better by using it as a part of an optical anchor system.

For longitudinal element alignment the line-of-sight (LOS) monitoring system is also suitable [51]. It uses several LED (laser)-lens-detector systems, with the LEDs mounted on the first object, the lenses on a second one, and the detectors on the third element. The precision expected with such a system is at micrometer level and hence highly sufficient to perform the task.

Industrial products for linear positioning systems with micrometer accuracy and excellent repeatability are widely offered. For example, the linear motor ultra stages from the Bayside Motion Group [52], utilizes a non-contact optical encoder, integrated directly into the stage footprint. The encoder tape scale is mounted upside-down and referenced directly off the bearing surface, eliminating any able error and protecting it from any debris. The encoder read head is mounted inside the stationary base, eliminating moving wires. Another example is given in Tab. 17, where some specifications for measurement sensors from the SMPR CONTROLE company [53] are summarized. But in many cases, additional design and manufacturing investment is needed to adapt commercially available products to the specific conditions for the LC energy spectrometer.

Main specification	**P9010**	**P9015**	**P9030**
Measuring range	10 mm	15 mm	30 mm
Measuring accuracy	+/- 0.75 microns	+/- 1 micron	+/- 1.25 microns
Measuring force	0.57 - 1.47N	0.73 - 1.68N	0.69 - 2.41N
Clamping	8h6	8h6	8h6
Plunger guide	Linear bearing	Linear bearing	Linear bearing
Measuring speed	1 m/s	1 m/s	1 m/s
Total weight	155 g	160 g	195 g

Table 17: Specifications of sensors from SMPR CONTROLE (France).

Transverse alignment and positioning of the BPMs are required at nanometer-scale precision. Alignments with $\leq$50 nm precision can be achieved with e.g. piezoelectrical devices or flexible bearings, a promising alternative [54]. Flexible bearings rely on the elastic properties of matter allowing for several advantages and, if combined with adequate actuators and sensors, ultra-high position resolution is achievable.

Also, nanometer-scale position performance of the BPMs can be realized with optical decoders [55]. An encoder consists of a scale and scanning device, that reads off the scale. Exposed linear encoders operate with no mechanical contact between the scanning head and the scale. This eliminates any mechanical backlash or hysteresis. The measuring standard for all exposed linear encoders is a phase grating applied to a carrier of steel or glass. Digital Readouts (DRO) are used for displaying the linear position when used in conjunction with HEIDENHAIN encoders [56]. DROs are available with one to four display positions with resolutions from 10 μm down to 5 nm. Typical functions available include distance-to-go, min/max display, program storage, RS-232-C output, tool memory, datum shift, and graphic screens. Parameters of HEIDENHAIN linear encoders are presented in Tab. 18.

Main specification	**LIP481**	**LIP581**	**LIP382**
Measuring range	10 - 420 mm	70 - 1440 mm	70 - 270 nm
Measuring accuracy	1 μm – 5 nm	1 μm – 50 nm	1 nm
Output signal	AC 1 V or TTL	AC 1 V or TTL	AC 1V or TTL
Period of signal	2 μm	4 μm	128 nm
Reference point	1	1 or fixed dist.	-

Table 18: Parameters of HEIDENHAIN linear encoders.

In general, a well-chosen network of precision micromovers and position sensors has the potential to achieve the tight tolerances for the BPMs. During alignment stages and long-term measurements the instruments involved in the network should provide continuously information to a computer system which, following a statistical analysis, calculates the actual position of each component, and then deduces and controls any movements to be made. Products with nano-scale accuracy exist, but such devices have not yet testet in a system such as this.

For the spectrometer performance the coplanarity of the analyzing magnet is also essential, because a rotation of the magnetic plane can shift the beam in the horizontal and vertical direction. For the control of the coplanarity of the magnet a system similar to the one used at HERA detectors is feasible [57]. It would be sufficient to mount CCD sensors on the analyzing magnet.

Besides careful mechanical alignment of the spectrometer elements, beam-based alignment procedures are also of importance. For example, in order to make a successful absolute energy determination, a 'straight line' reference is required, corresponding to the beam trajectory for zero-magnetic field on the magnets. The deviation of the position of the beam from this straight line gives the bend angle directly. In addition, monitor repositioning and recalibration between 'straight line' calibration and beam energy measurements is avoided, if a BPM linearity range of about ± 2.5 mm can be realized. Aligning the BPMs off the straight line with 0.4 to 2.5 mm for monitors 1 to 4 and with 2.5 to 0.4 mm for monitors 5 to 8, see also Fig. 1, ensures for beam energy measurements beam passing at similar (modulus) offsets to the BMP center.

A further benefit of passing the beam at large monitor offsets consists of a dipole mode signal which is at least several hundred times larger than the beam-angle signal. Consequently, no special care is required to remove or suppress the beam-angle noise. However, the possibility of a 'switching' spectrometer with positive and negative bend angle and difference measurements between them, which may cancel some systematic errors, is ruled out for such a 'fixed' BPM position scheme.

Postion deteriorations due to thermal effects on the spectrometer elements will be minimized by temperature stabilization circuits and selection of materials with small temperature expansion coefficients for the critical parts.

The bunches of the beam jitter in position and angle when entering the analyzing magnet. Typical position and angular variations were estimated to 10 μm and 30 nrad, repectively. Since the total path length of the beam within the analyzing magnet depends on the jitter, deterioration of the beam energy precision is possible. Using for example 30 μm and 50 nrad for position and angular jitter in horizontal and vertical direction simultaneously, an additional uncertainty of 0.092 ppm is expected for the longitudinal field integral. This value is negligible in comparison to the total anticipated field integral uncertainty of 20 ppm. For large beam jitter the BPMs measure the magnet's entrance and exit points of the beam with great reliability, so that path integral determination for individual bunches is possible. The dynamic range of the monitor electronics is adequate to perform such measurements.

If the spectrometer has to be realized as the 50 m long small-angle device located close to the IP, the magnets and the BPMs should be (preferably) mounted on individual girders, e.g. on honeycomb support structures with no structural resonances below 230 Hz. Due to the imperative position requirements needed in this case, relative vibrations between the BPMs have to be damped to a negligible level. Basically, active damping devices, so-called damping links, might be useful to attenuate surviving vibrations. Commercial stabilization products, for example the STACIS 2000 system from TMC [58] which consists of three to four independently stabilized support feet, can be utilized for this purpose.

Besides such a stiff sytem, a soft pneumatic system [59] with somewhat less damping performance seems also feasible. The whole device is essentially floating on a cushion of air which decouples the magnets/BPMs from the ground. Further work is however needed to investigate stability, alignment and enviroment issues in order to meet the stringent precision requirements for the small-angle spectrometer option.

3.6.3 The Control System of the Spectrometer

A reliable control system is important for a successful commissioning and operation of the energy spectrometer. The main tasks of such a system can be summarized as follows:

- stabilization and alignment control of the spectrometer elements,
- control of the magnetic fields and the electronics of the BPMs,
- measurement of the B-fields and the beam position in the BPMs,
- remote control of all relevant instrumentations,
- transfer of data for bunch related beam energy determination to the detector DAQ system,
- access to data from other systems.

The control system of the spectrometer could be formally divided into:

- a local system for monitoring the magnets, BPMs, alignment system, temperature circuits, including remote control
- a system to buffer and transfer the data to the main detector DAQ system, including access to data of other systems.

The main sources of significant information for the control system are presented in Tab. 19.
The total information flow rate is not critical for modern measurement instrumentations and computers. The networked protocol IEEE 488 possesses properties required to create a measurement system. Remote control of instruments, data handshake for reliable operation and real-time response are the main features of such a protocol. A preliminary schematic view of the

Device	N	Bits	Rate	To event label
Hall magnetometer and coils	6	16	1 Hz	+
NMR magnetometer	9	32	1 Hz	+
BPM sensors	10	18	5Hz x 2820 with 300 ns spacing	+
BPM step drivers	2	16	$\sim$ 1per day	+
SR detector, if applied	2	32	5Hz x 2820 with 300 ns spacing	+
Alignment modules	4	16	1 Hz	-
Temperature circuits	6	16	0.1 Hz	-
			$\sim$ 800Kb/sec	

Table 19: Sources of data for the control system.

system is shown on Fig. 25. The information from the BPMs needs buffering, denoted as 'Buf' in Fig. 25, due to the high information flow rate during a LC pulse of about 2800 bunches.

For the transfer of the data to the external DAQ system, Ethernet and related network using TCP/IP protocol are appropriate. Software development should be based on new industrial methods and standards. A modular design of the software is required to allow for flexibility (adaption of new standards and products) and should be in line with analogous develpments of control systems for the linac and other diagnostic tools.

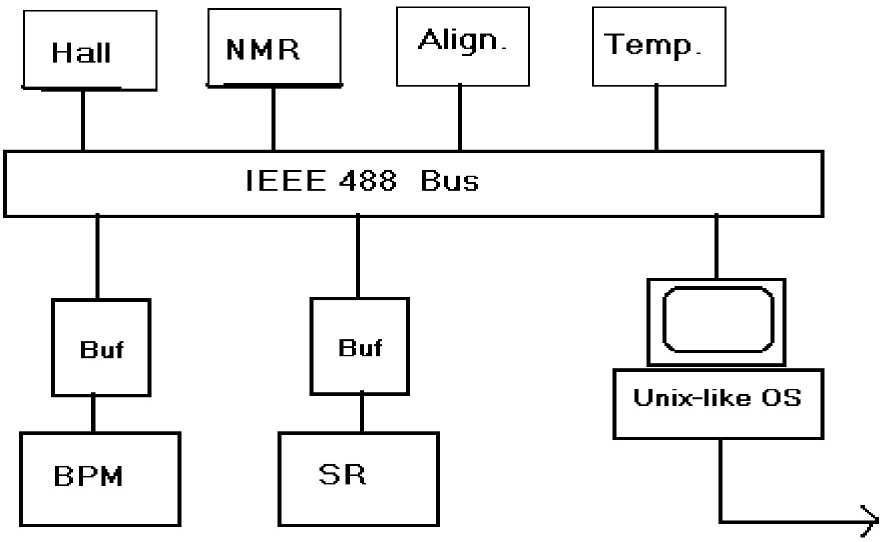

Figure 25: The schematic view of the control system.

4 Cost Estimates

4.1 Magnet Costs

Preliminary cost estimation of the magnet system for one spectrometer is summarized in Tab. 20. The estimation was done under the assumptions

- the design of the magnetic system will be carried out in LNP JINR;

- manufacturing of the magnets will be realized in JINR main experimental shops;
- manufacturing of the magnetometer equipments will be done in LNP JINR;
- for magnetic field measurements, the measuring table stand installed in LNP JINR will be used (with some modifications);
- laboratory measurements of the fields will be carried out in LNP JINR;
- techniques for field measurements in situ are included.

The estimated cost of the spectrometer magnets include experience with magnets already built or are presently under construction at other laboratories. Any cost evolution between now and the time of construction of the magnets is not taken into account.

Sub-system	Analyzing M.	Ancillary M.	Components included
Design drawings	3	2	
Tooling	4	5	
Material	7	2.5	yoke steel, copper conductor, insulation
Production	9	11	coils, yoke, ancillaries, magnet assembly
Measurement devices	50		NMR teslameter with probe multiplexer and 4 probes, Hall digital teslameter, digital integrator with probe coils and moving wire probe, digital multimeter, PC, temperature probe interface and 50 sensors, laser interferometer, mechanics for moving wire probe
Magnet tests and commissioning	50	10	magnet tests and commissioning, modernization of mechanics and control, software, stand assembly with tests and commissioning, field measurements, documentation and manuals
Power supplies	15	11	
Water cooling system	10		
Commissioning without beam	4		
Sum	**∼145**	**∼35**	

Table 20: Preliminary cost estimation for the magnets of one spectrometer.

4.2 BPM Costs

Cost estimations for 10 BPMs include material costs, the analog read-out electronics, the ADCs, the cooling system and the cables to transfer the 5.5 GHz signals to the electronic racks, assumed to be located 40 m away. Since no commercial ADCs with properties as needed are offered by industry, only a rough guess for their price could be made. Tab. 21 summarizes the costs. Some prices for sub-systems have been estimated based on experience with the test facility TTF and specific R&D prototype developments.

4.3 Costs for Stabilization, Alignment and the Control System

The cost estimation of the key elements for stabilization, alignment and the control system are summarized the Tab. 22. The numbers given were estimated by following examples of similar

Sub-system	Cost [kEUR]	Components included
monitors	35	monitor material, flanges, feedthrough feedthroughs, UHV-sealing
electronics	150	two types of filters, mixer, amplifier, limiter, hybrid, limiting amplifier, power supplies
ADCs	40	
cables	80	
cooling system	12	
Sum	**~320**	

Table 21: Preliminary cost estimation for 10 BPMs.

systems constructed or are being under construction. If available, offers of industry were taken into account. According to experiences from the past there is room for cost optimization due to significant decrease in price for most components needed at the time of construction. The estimated costs do not include processing and manpower costs.

Element	Number	Price (KEuro)	Cost(KEuro)
Computer	3	4	12
Positioning table	4	5.0	20
Controller for the table	4	3.0	12
Position sensors	8	0.5	4
Submicron position sensors	10	2.0	20
Control module for the sensors (PROMUS4C)	2	1.5	3
Control module for the submicron sensors	6	3.0	18
FSI modules	8	4.0	32
FSI controller	2	2.0	4
LOS modules	2	3.0	6
LOS controller	2	2.0	4
Temperature controllers	3	5.0	15
IEEE488 interfaces	8	0.5	4
Ancillary equipment: materials, cables, crates etc.			20
Sum			**~ 200**

Table 22: Cost estimation for stabilization, alignment and the control system.

The total investment costs for two BPM-based energy spectrometers including magnets, BPMs with electronics, survey, alignment and positioning devices as well as the control system are estimated to be about 1.4 million EUR. This number does not account for possible price evolution between now and the time of construction, so that room for cost optimization exists. It does not include costs for manpower. We assume that the manpower required for the various parts of the project will be supplied by the existing manpower in the collaborating institutes.

5 Summary and Conclusion

The physics program at a high-energy e^+e^- linear collider requires to measure the beam energy with a precision of $\Delta E_b/E_b \simeq 1 \cdot 10^{-4}$ or better. This demand is about a factor 10 more stringent compared to results achieved so far. It is essentially a technical challenge and requires solutions with nanometer-scale stability and resolution.

The canonical method for beam energy determination relies on a BPM-based energy spectrometer located upstream of the collision point. A linear collider utilizing the TESLA technology with its large bunch spacing allows for bunch related energy measurements on both the electron and positron sides. Dedicated assessment of E_b from the spectrometer is essential to deduce the effective center-of-mass energy $\sqrt{s}$ at the IP, which is directly related to physics quantities to be measured with so far unprecedented accuracy. It is worth to mention that no energy width measurement is possible with a BPM-based spectrometer.

The basic layout of the spectrometer as shown in Fig. 1 involves one analyzing (or spectrometer) magnet and two ancillary magnets. Three or four high-precision BPMs are proposed to be located in each lever arm of 10 m length. Absolute position accuracy of the monitors should be close to 200 nm. Additional BPMs upstream and downstream of the chicane constrain the external particle trajectories. The uncertainty of the field integral of the analyzing magnet is required to be $\Delta B/B \simeq 2 \cdot 10^{-5}$. A compact version for the spectrometer with an energy independent bend angle of 1 mrad is proposed in this report. It is strongly favoured compared to an option with a ten times smaller bend angle and 50 m in length positioned close to the IP. If for reasons of emittance dilution the spectrometer must be located close to the IP, a non-zero crossing angle design of the linear collider is strongly recommended.

High precision beam position monitors combined with precise information of the field integral of the analyzing magnet are prerequisites to achieve the anticipated beam energy accuracy. Other important issues are related to dedicated survey and alignment procedures as well as to stabilization and control systems over long periods.

A BPM with a novel coupling scheme and appropriate waveguides together with a TM_{010} sensor (reference) cavity was designed and tested in a test bench and with beam. Excellent suppression of the monopole mode of at least 100 dB was observed. A position resolution of 300 nm was measured over a displacement range of 100 μm, which is consistent with the demand of 100 nm if in particular improved read-out electronics will be employed.

A concept for the signal processing circuit has been presented. A first and preliminary realization using available commercial components was applied at the test bench and for measurements with beam. Necessary improvements were fixed in order to achieve an intrinsic 100 nm position uncertainty with a large dynamic range. Further R&D studies call for a larger linearity range up to ± 2.5 mm. Suppression of the beam-angle signal due to an inclined beam within the BPM is desirable. In order to keep the beam-angle signal to a relatively negligible level we propose a fixed, well-defined positioning of the BMPs. Within such a scheme, beam passing occurs at large ($\gtrsim 0.4$ mm) offset within the monitor resulting to a huge TM_{110} displacement signal. Also, shorten the length of the BPM and/or accounting for the 90 degree phase difference between the position and beam-angle signals within the electronics helps to suppress the beam-angle signal.

In summary, we recommend to follow this type of BPM as a most promising candidate for our purpose. Among various types of monitors, only the RF cavity BPM has the potential to achieve nanometer-range resolution and a center accuracy at the micrometer level.

Warm magnets with ferromagnetic cores are proposed for the spectrometer. Measurements at different nominal beam energies (between 45 and 400 GeV) are intended to be performed at approximately constant bend angle of 1 mrad by adjusting the B-fields of the magnets.

According to experiences achieved at SLAC, CERN and CEBAF, warm magnets possess several advantages. Relying on similar designs for the spectrometer magnets and accounting for similar performances (manufacturing tolerances, material impurities etc.) a field integral uncertainty of $\Delta B/B \simeq 2 \cdot 10^{-5}$ should be achievable.

Basic layouts of the analyzing and ancillary magnets are presented and their technical parameters are specified. Also, based on detailed computer model simulations, magnet fabrication tolerances and requirements on the magnet material are derived. Important for high precision B-field achievements are temperature stabilization of the analyzing magnet and its monitoring using a water cooling circuit. Hysteresis effects and zero-field adjustment are believed to be under control by utilizing dedicated procedures.

Commercially available power supplies fulfill all necessary criteria. Therefore, no additional R&D effort is necessary.

The uniformity region of the magnets (defined by 20 ppm relative uncertainty limits) is expected to be 5 mm or larger, which is suitable for spectrometer working procedures without transverse adjustment. Devices for best B-field determinations should be used in the laboratory and in situ. Laboratory measurements should be performed by NMR probes in the main field region and Hall probes in the end region, while utilization of search coils is suggested as a complementary second method. Field measurements in situ are proposed to utilize reference NMR probes at two fixed points and the moving wire technique. Systematic errors derived from different B-field measurements based on custom designed devices are estimated of being below 20 ppm.

Vibrations are generated by ground motion (seismic and culture noise) and possibly by the accelerator complex itself. To achieve the necessary accuracy of beam energy measurements, vibrations have to be strongly damped. We propose to utilize a common 25 m long girder on which the spectrometer components are mounted. Any surviving vibration might be further attenuated to nanometer-scale sizes by using active damping devices commercially available. Alignment of the spectrometer as a whole within the beam delivery system is achieved with the global linear collider alignment system. The stringent alignment and positioning demands for the BPMs within the spectrometer system need novel approaches to achieve a nanometer-scale level. Developments on e.g. frequency scanning interferometry in combination with Michelson interferometry could fulfill the specifications.

A reliable control system is important for a successful commissioning and operation of the energy spectrometer. The basic requirements on such a system, including remote control and access to data from other systems, are manageable. Modular design of software is required to allow for wide flexibility.

It is very important that an energy spectrometer located within the beam delivery system should be taken into account during the design phase of the beam optics. Free space of typically 30-50 m has to be reserved for that purpose. Interferences of the spectrometer magnets with other beamline systems should be avoided, but needs to be addressed. In particular, possible impacts on beam emittance dilution have to be carefully evaluated.

In this report operational issues were not considered. They should be discussed in the overall context of running the LC and the physics requests. Basically, our approach allows for an absolute bunch-by-bunch energy determination over the center-of-mass energy ranging from the Z pole to about 1 TeV.

Of importance is also the possibility of cross-calibration of the energy determined from the spectrometer against other methods. The unprecedented accuracy of the resonance depolarization approach as applied in circular machines is excluded for linacs. Some novel suggestions like Møller scattering [60], spin precession [61], synchrotron light measurements [62] and the resonance absorption method [63] should be evaluated in detail. The technique based on radiative return events using the precisely known Z boson mass or Z- and W-pair production might also be useful. To arrive at some consensus within the next years as to which methods are most promising is highly desirable.

We would also like to mention that similar LC beam spectrometer activities are ongoing in other regions, see e.g. [64].

6 Acknowledgments

We are grateful for the support of N. Russakovich and A. Olshevsky during the course of this study. The authors are indebted to F. Kircher and P. Vernin for valuable advice and many informations on the spectrometer magnets and field measurement techniques. We would like to thank the operation crew for the very good performance of the ELBE linac in Rossendorf and P. Michel as well as P. Evtushenko for assistance and support. We acknowledge the Heinrich-Hertz-Institut for generous leave of 5.5 GHz electronic components and the Hahn-Meitner-Institut for brazing the copper BPM prototype.

References

[1] TESLA Technical Design Report, Part II, The Accelerator, DESY 2001-011, ECFA 2001-209, hep-ph/0106315.

[2] R. Assmann et al., CERN-PH-EP-2004-032, CERN-AB-2004-030 OP, hep-ex/0410026;
G. Wilkinson, contribution to the 26th Advanced ICFA Beam Dynamics Workshop on Nanometer Size Colliding Beams, Lausanne, Switzerland, 2-6 September 2002;
B. Dehning, Status of the LEP2 Spectrometer Project, Proceedings of EPAC 200, Vienna, Austria, 2000.

[3] D. Peralta, M. Martinez and R. Miquel, contribution to the Proceedings of the International Workshop on Linear Colliders (LCWS99), Sitges, May 1999.

[4] S. Heinemeyer et al., hep-ph/0306181.

[5] see e.g. A. Straessner (for the LEP Collaboratiuons), Proc. of the XXXIXth Recontres de Moriond, 2004, Electroweak Interactions and Unified Theories; hep-ex/0405005.

[6] P. Garcia, W. Lohmann and A. Rasperezca, TESLA note LC-PHSM-2001-054.

[7] G.W. Wilson, TESLA note LC-PHSM-2001-009.

[8] P.C. Rowson and M. Woods, SLAC-PUB-8745, hep-ex/0012055;
R. Hawkings and K. Moenig, DESY 99-157, 1999.

[9] e.g. S. Boogert, contribution at the ECFA LC Workshop, Montpellier, 2003.

[10] W.D. Woodley and P.E. Emma, SLAC-PUB 8581, 2000.

[11] V. Gharibyan, N. Meyners and K.P. Schüler, LC-DET-2001-047.

[12] H.J. Schreiber, Muon Background, Talk at the Workshop of the 2nd ECFA/DESY Study of Physics and Detectors for a Linear Electron-Positron Collider, Hamburg, Germany, 2000.

[13] B. Dehning, Status of the LEP2 Spectrometer Project, Proceedings of EPAC 2000 , Vienna, Austria, 2000.

[14] F. Roncarolo et al., High Accuracy Field Mappings with a Laser Monitored Travelling Mole. In Proceedings of EPAC 2000 , Vienna, Austria, 2000.

[15] J. Prochnow, The LEP Energy Spectrometer, Diplomarbeit in Physik, RWTH Aachen, September 2000.

[16] F. Roncarolo, High Accuracy Magnetic Field Mapping of the LEP Spectrometer Magnet, Thesis, Academic Year 1999-2000.

[17] J. Kent et al., Precision Measurements of the SLC Beam Energy, SLAC-PUB-4922, LBL-26977, 1989.

[18] S. Watson et al., Precision Measurements of the SLC Reference Magnets, SLAC-PUB-4908, LBL-26956, 1989.

[19] M. Levi et al., Precision Measurements of the SLC Spectrometer Magnets, SLAC-PUB-4654, 1989.

[20] F. Gougnaud et al., Controls for High Precision Beam Energy Determination at CEBAF, HALL A: The ARC Project. ICA LEPCS, 1999, Trieste, Italy.

[21] F. Kircher et al., Reference dipole measurement for CEBAF beam energy determination, Proc. of MT-15 Conference, 1279-1282, Beijing, China, 1997.

[22] F. Kircher et al., High Accuracy Field Integral measurement for CEBAF Beam Energy determination, Proc. of MT-16 Conference, Jacksonville, Florida, USA, 1999.

[23] N.A. Morozov and H.J. Schreiber, Magnetic field calculations for the technical proposal of the TESLA spectrometer magnet, JINR communication - E9-2003-65, Dubna, 2003 and **Meeting on BPM-based Beam Energy Spectrometer**, March 17/18, 2003 in DESY Zeuthen, **http://www-zeuthen.desy.de/e_spec/Morozov.pdf**.

[24] N.A. Morozov, The preliminary estimation of the parameters for the TESLA spectrometer magnet, Internal report, LNP JINR, Dubna, 2002.

[25] N.A. Morozov, Calculations on optimization of the parameters for the TESLA spectrometer magnet, Internal report, LNP JINR, Dubna, 2003.

[26] N.A. Morozov, Calculations on determination of the influence of manufacturing unaccuracy and temperature effects on quality of the magnetic field for the TESLA spectrometer magnet, Internal report, LNP JINR, Dubna, 2003.

[27] N.A. Morozov, Calculations for estimation of the parameters for the TESLA spectrometer ancillary magnets, Internal report, LNP JINR, Dubna, 2003.

[28] N.A. Morozov, Properties of synchrotron light for the TESLA spectrometer magnets, Internal report, LNP JINR, Dubna, 2003.

[29] N.A. Morozov, Calculations of some additional tolerance effects for the TESLA spectrometer magnet, Internal report, LNP JINR, Dubna, 2003.

[30] N.A. Morozov, Magnetic field calculations for the TESLA spectrometer ancillary magnet (in the version of 1/2 of the analyzing one) by the MAFIA code, Internal report, LNP JINR, Dubna, 2003.

[31] N.A. Morozov, Magnetic field calculations for the TESLA spectrometer ancillary magnet (in the preferable compact version) by the MAFIA code, Internal report, LNP JINR, Dubna, 2003.

[32] N.A. Morozov, Magnetic field calculations for the TESLA spectrometer main magnet by the 3D MAFIA code, Internal report, LNP JINR, Dubna, 2003.

[33] N.A. Morozov, Review of the magnetic measurement technique (experience of the SLC, LEP, CEBAF), **Meeting on BPM-based Beam Energy Spectrometer**, October 13-14, 2003, Dubna,
http://www-zeuthen.desy.de/e_spec/morozov_field_meas.pdf.

[34] N.A. Morozov, Proposals for the magnetic field measurement technique of the TESLA spectrometer magnets, Internal report, LNP JINR, Dubna, 2003.

[35] N.A. Morozov, Review of the progres in the 2D and 3D magnetic field simulation for the TESLA spectrometer magnets, **Meeting on BPM-based Beam Energy Spectrometer**, October 13-14, 2003, Dubna,
http://www-zeuthen.desy.de/e_spec/morozov_magnets.pdf.

[36] A. Temnykh, Nucl.Instr. and Methods, A 399 (1997) 185.

[37] N. Morozov, private information.

[38] A. Liapine, Strahllagemonitor fuer das TESLA-Spektrometer, Thesis, TU-Berlin, Dezember 2003 (in German).

[39] T. Shintake, Proposal of Nanometer Resolution Beam Position Monitor, KEK preprint 98-188, November 1998.

[40] W. Schnell, Common-mode Rejection in Resonant Microwave Position Monitors for Linear Colliders, CERN-LEP-RF/88-41 CLIC Note 70, (1988).

[41] R. Johnson et al., An X-Band Cavity for a High Precision Beam Position Monitor, Proceedings DIPAC2003, Mainz, Germany, 2003;
R. Johnson et al., Cavity BPMs for the NLC, SLAC-PUB-9211, May 2002.

[42] W. Bruns, The GdfidL Electromagnetic Field Simulator, http://www.gdfidl.de.

[43] U. Hahn et al., Nucl. Instr. and Meth. A 527 (2004) 240;
TESLA Report, TESLA-FEL 2003-04, 2003.

[44] see e.g. Proceedings of the 7th International Workshop on Accelerator Alignment, SPring-8, 2002.

[45] e.g. A. Seryi and T. Raubenheimer, SLAC-PUB-8595, 2000.

[46] R. Brinkmann and J. Rossbach, NIM Ph.Res. A 350 (1994) 8.

[47] H. Matsumoto et al., Proceedings of EPAC 2002, Paris, France;
KEK- Preprint-2002-49.

[48] T. Mattison et al., 26th Advanced ICFA Beam Dynamics Workshop on Nanometer Size Colliding Beams - Nanobeam 2002, p.81, CERN-Proceedings-2003-001, 2-6 Sept. 2002, Lausanne, Switzerland.

[49] J. Frisch et al., hep-physics/0112042.

[50] P. Coe et al., 26th Advanced ICFA Beam Dynamics Workshop on Nanometer Colliding Beams - Nanobeam 2002, p.143, CERN-Proceedings-2003-001, 2-6 Sept. 2002, Lausanne, Switzerland;
P. Coe, D.Phil. Thesis, University of Oxford, 2002.

[51] A. Mitra, D.Phil. Thesis, University of Oxford, 2002.

[52] Bayside Motion Group, 27 Seaview Blvd., Port Washington, NY 11050, USA.

[53] SMPR CONTROLE, 22, avenue des vieux moulins 74000 Annecy FRANCE .

[54] S. Henein et al., 26th Advanced ICFA Beam Dynamics Workshop on Nanometer Colliding Beams - Nanobeam 2002, p.103, CERN-Proceedings-2003-001, 2-6 Sept. 2002, Lausanne, Switzerland.

[55] R.K. Heilmann et al., IEEE Conference on Nanoscale Devices and System Integration, Miami, Florida, USA, 2004 (submitted to 'Nanotechnology').

[56] HEIDENHAIN production catalog, www.heidenhain.com.

[57] V. Shiltsev et al., *Measurements of Ground Vibrations and Orbit Motion at HERA*, DESY-HERA-95-06, 1995.

[58] R. Assmann et al., CERN-AB-2003-011 ABP, CERN, 2003.

[59] R. Assmann et al., 26th Advanced ICFA Beam Dynamics Workshop on Nanometer Size Colliding Beams - Nanobeam 2002, p.87, CERN-Proceedings-2003-001, 2-6 Sept. 2002, Lausanne, Switzerland.

[60] P. Galumian et al., Nucl. Instrum. Meth., A327 (1993) 269;
C. Checchi, J.H. Field and T. Kawamoto, Nucl. Instrum. Meth. A385 (1997) 445.

[61] V.I. Telnov, 26th Advanced ICFA Beam Dynamics Workshop on Nanometer Size Colliding Beams - Nanobeam 2002, p.159, CERN-Proceedings-2003-001, 2-6 Sept. 2002, Lausanne, Switzerland.

[62] E.M. Syresin, private communication.

[63] D.P. Barber and R.A. Melikian, Proceedings of EPAC2000, Vienna, 2000;
R.A. Melikian and D.P. Barber, DESY 98-015 (1998) and hep-ph/9903007.

[64] **http://www.slac.stanford.edu/xorg/lcd/ipbi/energy/Energy_Spectrometer.html.**